RSC Advances

ROYAL SOCIETY OF CHEMISTRY

www.rsc.org/advances

Table of Content

Fluorescence sensing and intracellular imaging of Al^{3+} ions by using naphthyl appended sulfonamide chemosensor : structure, computation and biological studies

Sudipa Mondal, Durbadal Ojha, Tapan Kumar Mondal, Debprasad Chattopadhyay and Chittaranjan Sinha*

Naphthyl appended sulfonamide Schiff base (HL), an antimicrobial nontoxic agent, serves as a fluorogenic sensor to Al^{3+}, LOD 33.2 nM and is used for living cell imaging.

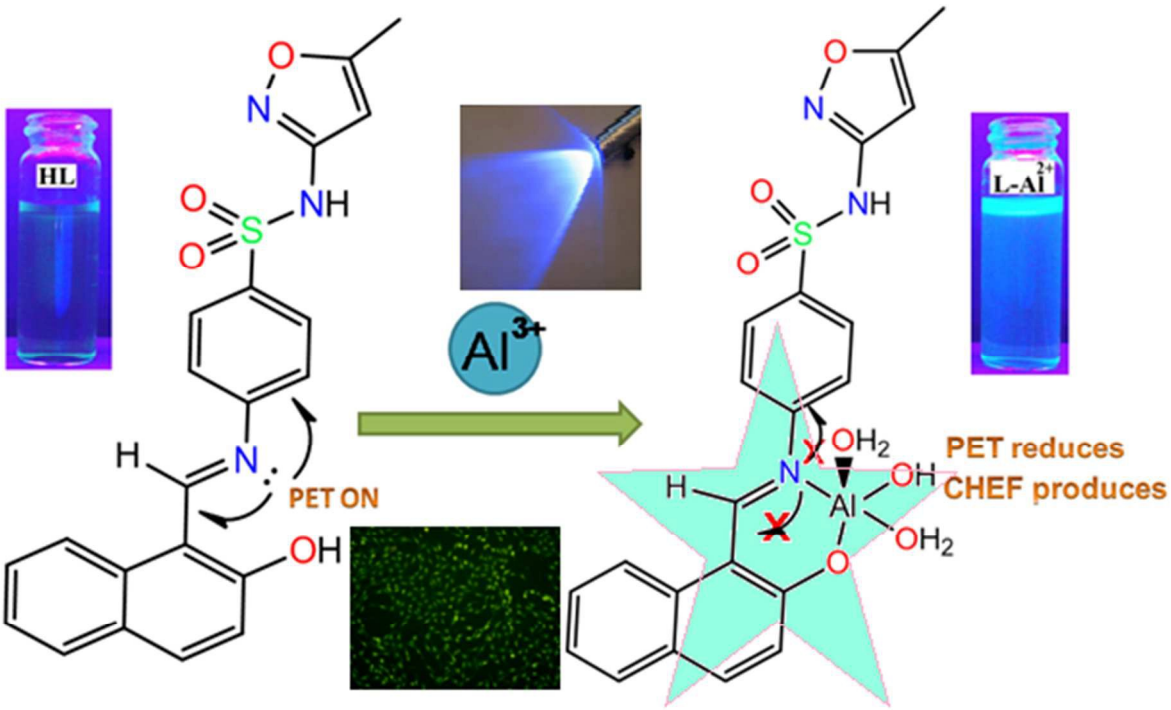

Fluorescence sensing and intracellular imaging of Al^{3+} ions by using naphthalene based sulfonamide chemosensor : structure, computation and biological studies

Sudipa Mondal[a], Anup Kumar Bhanja[a], Durba Ojha[b], Tapan Kumar Mondal[a], Debprasad Chattopadhyay[b] and Chittaranjan Sinha[a*]

A naphthalene based sulfonamide Schiff base, (E)-4-(((2-hydroxynaphthalen-1-yl)methylene)amino)-N-(5-methylisoxazol-3-yl)benzenesulfonamide (HL) has been found to be a flourescence turn-on probe for selective detection of Al^{3+} in aqueous system. Structure of the probe has been established by FTIR, ^1H NMR, mass spectra and X-ray single crystal study. The probe has shown 24 times flourescence enhancement in presence of Al^{3+}. The limit of detection (LOD) obtained by 3σ method is 33.2 nM. The probable co-ordination environment of L-Al^{2+} complex has been supported by mass spectral data and DFT computational study. By TD-DFT calculation UV-Vis spectra of HL and L-Al^{2+} complex has been predicted and that has well correlated with experimental data. Cell imaging study reveals that the probe can be used for the intracellular detection of Al^{3+} in cultured Vero cell. Antimicrobial activity of HL has also been evaluated and probable mode of binding inside the DHPS cavity has been predicted by docking study. This sensor is unique with reference to two other predecessors because of its bio-compatibility of sulfonamide derivative and nonmutagenicity.

[a]Department of Chemistry, Jadavpur University, Kolkata – 700 032, India, c_r_sinha@yahoo.com, fax-+91-2414-6584

[b]ICMR Virus Unit, I.D. & B.G. Hospital, Beliaghata, Kolkata-700032, India

Introduction

Aluminium, the third most abundant metal in the earth's crust (8% of its mass), has remarkable ability to resist corrosion and is a useful structural component of electronic and electrical gadgets, building materials, packaging stuff etc. Elevated aluminium causes neurotoxicity[1] and has been manifested Alzheimer's[2] and Parkinson's[3] diseases, and hampers protein transportation in respiratory system, softening of bone, anemia in living beings. Al^{3+} interferes with the uptake of Ca^{2+} and results the growth retardation of living systems[4]. Besides, the toxicity of aluminium is a hazard towards aquatic life [5] and retards agricultural production in acidic soils [6]. Notwithstanding, the use of Al cannot be avoided in modern life. Therefore, there is a good chance of accumulation of Al^{3+} and toxicity towards human health. As a result, developing of new and practical multi signaling chemosensor for Al^{3+} is very important.[7-9] To date several techniques are available for detection of Al^{3+} including atomic absorption spectra[10], electrochemical detection,[11] mass spectrometry,[12] and ^{27}Al NMR technologies.[13]. Recently fluorescence spectroscopic technique has received worldwide interest because of selective, efficient, time saving, environmentally benign and low cost chemosensing property. Many fluorescent probes have been characterized and some have been used successfully in Al neurochemistry. Most of them have been developed based on quinoline[14-16], bipyridyl[17-18], coumarin[19-20], pyrazoline[21-22], tripyrrins[18] , BINOL[23], fluorescein[20-21], rhodamine[24-25] fluorophores. Functionalized Schiff bases are useful complexing agents and have been designed to incorporate fluorescent moiety for optical sensing of metal ions[26-28]. In this work, a sulfonamide based naphthol Schiff base, (E)-4-(((2-hydroxynaphthalen-1-yl)methylene)amino)-N-(5-methylisoxazol-3-yl)benzene sulfonamide (HL) is structurally characterized which shows high selectivity for Al^{3+} with low detection limit. Sulfonamides and their derivatives have

widespread use as antibacterial medicine and several sulfa drugs based receptors are also reported in literature for anion sensing[29-32]. The composition of the complex has been supported by spectroscopic data (IR, Mass, Job's plot, ^{1}H NMR). The DFT computation of optimized geometry of HL and the complex has been used to explain the electronic spectral properties. The practical applicability of the ligand (HL) has been tested in African green monkey kidney cells (Vero cells, ATCC, Manassas, VA, USA) for the determination of exogenous Al^{3+} ions by fluorescence cell imaging processes and the cell cytotoxicity of the probe has been examined by MTT assay. The antimicrobial activity of HL has also been examined against selected Gram-positive and Gram-negative bacteria which revealed that HL had moderate antibacterial activity (32-64 μg/ml). The mechanism of antimicrobial activity has been proposed by *in-silico* process of molecular docking of HL in the structure of DHPS protein.

Experimental

Materials and methods

Sulfamethoxazole was purchased from Hi-Media and 2-hydroxy naphthyldehyde was prepared from 2-naphthol following Duff reaction[33]. All other chemicals and solvents were of analytical grades and used without further purification.

Physical measurement

Melting points were determined on a melting Point machine apparatus using open capillary. The IR spectra (in KBr pellets) were recorded on a Rx-1 Perkin Elmer spectrophotometer in the range 4000-400 cm^{-1}. The ^{1}H and ^{13}C NMR spectra were recorded in DMSO-d_6 on Bruker 300 MHz FT-NMR spectrometer using TMS as internal standard. The mass spectra were recorded on a Water HRMS model XEVO-G2QTOF#YCA351 spectrometer. UV-Vis spectra were recorded on Lambda 25 Perkin Elmer spectrophotometer and emission spectra were measured in Perkin

Elmer LS55 fluorescence spectrophotometer at room temperature (298K). The fluorescence quantum yield was determined using anthracene as reference with a known quantum yield, ϕ_R = 0.27 in acetonitrile[34]. The experimental sample and reference were excited at same wave length, maintaining almost same absorbance and fluorescence were measured. Area of the fluorescence spectra were measured using the software available in the instrument and the quantum yield was calculated by following the formula

$$\phi_u / \phi_R = [A_u / A_R] \times [(Abs)_R / (Abs)_u] \times [\eta_u^{\ 2} / \eta_R^2]$$

where, ϕ_u and ϕ_R are the fluorescence quantum yield of the samples and reference; A_u and A_R are the respective areas under emission spectra of the sample and reference respectively. $(Abs)_R$, $(Abs)_u$ are the absorbance of sample and reference at the excitation wave length and η_u^2 , η_R^2 are the refractive index of the solvent used for the sample and the reference.

Elemental analyses were performed using a Perkin-Elmer 2400 Series-II CHN analyzer, Perkin Elmer, USA. elemental analyzer. Cell imaging study were executed using Zeiss Axiovert 40 CFL fluorescence microscope.

Synthesis of (E)-4-(((2-hydroxynaphthalen-1-yl)methylene)amino)-N-(5-methylisoxazol-3-yl)benzenesulfonamide (HL)

2-Hydroxynaphthaldehyde (0.2 g, 1.16 mmol) was dissolved in 15 ml of ethanol followed by the dropwise addition of ethanol solution of sulfamethoxazole (SMX) (0.3 g, 1.18 mmol in 10 ml) with constant stirring for 30 mins. The mixture was then refluxed for 2.5 hrs. The solution was then cooled to room temperature and allowed to evaporate slowly in air; an orange colored crystals of the precipitate of (E)-4-(((2-hydroxynaphthalen-1-yl)methylene)amino)-N-(5-methylisoxazol-3-yl)benzenesulfonamide (HL) deposited on the wall of the beaker. The crystals

were filtered and further recrystallized from hot ethanol. The purity of the product was checked by TLC; yield, 0.30 g (63%)

M.p., 244(2)°C. MS : m/z = 408.13; IR: 3458, 3066(O-H), 2960, 1624 (azomethine, -HC=N-), 1587, 1351, 1170, 1180 (-S=O of SO_2), 1090, 842, 742, 623, 574. ^{1}H NMR (300 MHz, DMSO-d_6): δ 11.46 (1H, s, OH), 9.60 (1H, s ,11-H); 8.49 (1H, d, J=8.4, 3-H); 7.96 (1H, s, 8-H); 7.92(3Hs, d, J=8.73, 14-H, 16-H, 4-H); 7.79 (2Hs, d, J=8.4, 13-H, 17-H); 7.56 (1H, t, J=7.56, 7-H); 7.38 (1H, t, J=7.4, 6-H); 7.00 (1H, d, J=9.2, 5-H); 6.17 (1H, s, 19-H); 2.29 (3Hs, s, -CH_3 at 15-C). ^{13}C NMR (300 MHz, DMSO-d_6): δ170.9 (18-C), 164.4 (2-C), 158.3(20-C), 157.4 (11-C), 153.8 (15-C), 148.8 (12-C), 138.9 (1-C), 136.8 (3-C), 133.5 (4-C), 132.2 (9-C), 129.5 (10-C), 128.8 (14-C,16-C), 127.3 (8-C), 124.7(5-C), 122.5 (7-C), 121.6 (13-C,17-C), 119.2 (6-C), 95.93 (19-C), 12.52 (CH_3 at 20-C). Anal. Calcd. for $C_{21}H_{17}N_3O_4S$ (407): C, 61.90; H, 4.21; N, 10.31%. Found: C, 61.30; H, 4.40; N, 10.58%. Figures are given in **Supplementary Material, Fig. S1 (Mass); Fig. S2 (IR); Fig. S3 (^{1}H NMR**); **Fig. S4 (^{13}C NMR).**

Synthesis of Al^{3+} complex of HL

To the solution of HL (0.1 g, 0.245 mmol) in 30 ml MeOH, $Al(NO_3)_3$. $9H_2O$ (0.1 g, 0.267 mmol) in same solvent (20 ml) was added drop wise with constant stirring. The yellow colored solution of HL turned colorless after complete addition of $Al(NO_3)_3$ and the solution was stirred for further 2 hours. The solution was allowed to evaporate slowly in air and gummy mass was extracted with CH_2Cl_2 and washed with water for several times. A light yellow mass was then dried in vacuuo and purity was checked by TLC prepared in alumina. A single band was eluted by chloroform-ethylacetate (1:1, v/v) and it was compared with TLC of HL under similar condition. Yield, 0.09 g (68%).

Light yellow sticky product was dried in vacuuo and MS (m/z) peak appeared at 486.17 (**Supplementary Material, Fig. S5**); which has supported the composition $[AlL(OH)(H_2O)_2](NO_3)$. The microanalytical data revealed that Calcd. (%): $C_{21}H_{21}AlN_4O_{10}$: C,45.99; H, 3.86; N, 10.22% and Found (%), C, 46.08; H, 3.75; N, 10.15%. The conductance data is very confusing; in ethanol the complex showed 1:1 conductivity (Λ_M, 106 $\Omega^{-1}cm^2mol^{-1}$). The FTIR spectrum also showed presence of a sharp band corresponding to free $\nu(NO_3)$ at 1370 cm^{-1} along with ν(C=N), $\nu(SO_2)$, ν(OH) appear at 1615, 1194 and 2950 cm^{-1} respectively (**Supplementary Material, Fig. S6**). The ^{1}H NMR spectrum of the complex (300 MHz, DMSO-d_6) shows δ 10.05 (1H, s ,11-H); 7.03 (1H, b, 3-H); 8.19 (1H, s, 8-H); 7.61 (3Hs, d, J = 8.33, 14-H, 16-H, 7-H); 6.78 (2Hs, d, J = 8.05, 13-H, 17-H); 7.46 (1H, t, J = 7.5, 6-H); 7.82 (1H, d, J = 8.5, 5-H); 6.09 (1H, s, 19-H); 2.31 (3Hs, s, -CH_3 at 20-C) (b, broad; s, singlet; d, dublet; t, triplet) (**Supplementary Material, Fig. S7**).

X-Ray Crystallography

The single crystals of HL (0.16 x 0.12 x 0.09 mm) were obtained by slow diffusion of mixture of dichloromethane with hexane solution (1:1, v/v) The X-ray crystal data were collected (**Table 1**) by Bruker Smart Apex II CCD Area Detector at 296(2) K. Diffraction were recorded with 2θ in the range $1.74 \leq \theta \leq 25.00°$ (HL)**.** Fine-focus sealed tube was used as the radiation source of graphite-monochromatized MoK/α radiation (λ = 0.71073 Å). Data were corrected for Lorentz and polarization effects and an empirical absorption correction in the *h k l* range for $-9 \leq h \leq 9$; $-11 \leq k \leq 11$; $-14 \leq l \leq 15$ for HL. The absorption corrections were done by the multi-scan technique[35]. All data were corrected for Lorentz and polarization effects, and the non-hydrogen atoms were refined anisotropically. The structure was solved by direct methods with SHELXL-

97 [36] and refined by full-matrix least-squares techniques on F^2 using the SHELXS-97 [36] program with anisotropic displacement parameters for all non-hydrogen atoms. The ORTEP-3 [37] was used within WinGX [38] to prepare figures and tables for publication. Hydrogen atoms were constrained to ride on the respective carbon atoms with isotropic displacement parameters equal to 1.2 times the equivalent isotropic displacement of their parent atom in all cases of aromatic units.

Computational details

Electronic structure optimization of the ligand and Al complex were carried out in B3LYP [39] using Gaussian09 software[40] package. The 6-31G(d, p) basis set was assigned for all the elements except sulfur. For sulfur atom 6-31+G(d, p) basis set was used. Theoretical computation for UV-Vis absorption spectral studies were done by time dependent density functional theory (TD-DFT)[41-43] in methanol conductor-like polarizable continuum model (CPCM)[44-46] using the same B3LYP level and basis set. Gauss sum[47] was used to calculate theoretical electronic spectra and molecular orbital contribution from groups or atoms.

Cell culture and cell imaging study

The Vero cells (African green monkey kidney cells, ATCC, Manassas, VA, USA) was grown and maintained in Dulbecco's modified Eagle's medium (DMEM, Gibco, USA), supplemented with 5–10% fetal bovine serum (FBS, Gibco, USA) in an atmosphere of 5% CO_2 at 37 °C. Vero cells monolayer (1.0×10^6 cells/ml) grown onto 6 well plates at 5% CO_2 for 24 h, were fixed with paraformaldehyde (4%) and blocked with 1% bovine serum albumin (BSA) in 0.1% phosphate buffered saline (PBS, pH 7.2)-triton X100 solution. The cells were washed with PBS, and then permeabilized with 0.1% triton X100 in PBS. The permeabilized Vero cells

monolayer treated with the compound (100 µg/ml) for 1 h at room temperature was then washed twice with PBS to remove the cell debris. After washing with PBS, the cells were added with $Al(NO_3)_3.9H_2O$ for 10 min, washed twice with PBS, and then the cells were observed under Axiovert 40 CFL inverted epifluorescence microscope[48].

Cell cytotoxicity assay

Cytotoxicity of HL on Vero cells were performed following the MTT ([(3-(4,5-dimethylthiazol-2-yl)-5-(3-carboxymethoxyphenyl)-2-(4-sulfophenyl)-2Htetrazolium)]) assay as per the protocol described earlier [49,50]. The cells seeded in 96 well plates were treated with different concentrations of HL and incubated for 24 hours in 5% CO_2 at 37 °C. For the MTT assay, thiazolyl blue tetrazolium bromide solution (100 µL; 1 mg/ml) in incomplete medium was added and this mixture incubated for 4 hours. After that, 100 µl of dimethylsulphoxide (DMSO) was added and the plates were rotate for 5 minutes. Optical density was recorded at 550 nm with DMSO as the blank. Percentage of cell viability was plotted against different concentrations of HL and the cells treated without any compound served as control.

Antimicrobial assay

(E)-4-(((2-Hydroxynaphthalen-1-yl)methylene)amino)-N-(5-methylisoxazol-3-yl)benzene sulfonamide (HL) was tested against Gram-positive (*S. aureus* ATCC21737, *Enterococcus facelis* ATCC 29212) and Gram-negative (*E. coli*, ATCC 25922, *S. typhi* MTCC734, *K. pneumonia* ATCC 714) bacterial strain. Minimum inhibitory concentration (MIC) values of HL and SMX were determined according to CLSI guidelines following broth microdilution method [51] and MIC data were recorded where no visible growth was observed. The bacterial growth and

culture conditions were examined as literature report [52] and all independent experiments were repeated three times.

Result and Discussion

Synthesis and formulation of probe

The condensation of 2-hydroxy naphthaldehyde with sulfamethozaxole (SMX) in ethanol under refluxing condition using 1:1 molar ratio (**Supplementary Materials**, **Scheme S1**) has synthesized (E)-4-(((2-hydroxynaphthalen-1-yl)methylene)amino)-N-(5-methylisoxazol-3-yl) benzene sulfonamide (HL). The mass spectral peak of HL appears at (m/z) 408.129 (**Supplementary Materials, Fig. S1**) (Mol weight, 407.44). The characteristic stretching vibrations of HL are υ(O-H), 3066 cm^{-1}; υ(C=N), 1624 cm^{-1}; υ(S-O), 1170 (sym) and 1351 (asym) cm^{-1} (**Supplementary Materials, Fig. S2**). The ^{1}H NMR spectrum of HL (DMSO-d_6) shows two higher frequency resonances at 11.46 ppm (δ(OH)) and 9.6 ppm (δ(CH=N); oxazolyl –Me signal appears at 2.29 ppm, the oxazolyl-H resonates at 6.17 ppm and four phenyl Hs exhibit two doublets at 7.92 ppm (14,16-H, J = 8.73 Hz) and 7.79 ppm (13,17-H, J = 8.70 Hz), naphthyl-Hs are assigned to 8.49-6.90 ppm. (**Supplementary Materials, Fig. S3**). The ^{13}C NMR spectrum (in DMSO-d_6) of HL is very complex and has been assigned on comparing with literature report[53] (**Supplementary Materials, Fig. S4**)..

The structure of HL has been confirmed by single crystal X-Ray diffraction measurements. The ORTEP plot of HL is shown in **Fig.1** and the selected bond parameters are listed in **Table 2.** The structure shows that the imine group (-CH=N-) binds naphtholato and SMX. The $–SO_2NH-$ bridges C_6H_4-CH=N- and methyl-oxazolyl units. The S=O bond length

(1.423(3), 1.433(3) Å)[53-55] in SMX and imine, -C=N-, bond length, C(11)-N(3) (1.327 Å)[56] are corroborated with literature data. The bond angle ∠O(2)–S(1)–O(1), 120.31°(17) appropriates to trigonal symmetry. Intramolecular and intermolecular hydrogen bonds such as O(4)-H(4)---N(3)-C(8) (H(4)---N(3), 1.71(6) Å; O(4)---N(3), 2.538(3) Å), ∠O(4)-H(4)---N(3), 152(8)°), O(4)-H(4)---N(2)-C(4) (H(4)---N(2), 2.03(4) Å; O(4)---N(2), 2.791(5) Å), ∠O(4)-H(4)---N(2), 164(3)°; symmetry, -x,-y,-z) give rise to the formation of an 1D tape and π---π interaction between sulfonamide phenyl ring and naphthyl ring of neighboring molecule (Cg(2)---Cg(3), 3.668(3) Å where Cg(2) : C(5)-C(6)-C(7)-C(8)-C(9)-C(10) and Cg(3), C(12)-C(13)-C(14)-C(15)-C(16)-C(21)) generates 2D supramolecular plane (**Fig. 2**). Relevant H Bonds are shown in *Supplementary material* (**Supplementary Material**, **Table S1**).

The structural parameters calculated from optimized structure using DFT computation technique are marginally elongated by 0.006 – 0.13 Å (bond lengths) and 0.5-2° (bond angles) (**Table 2**) from that of X-ray crystallographic data. Thus the optimized functions are useful to explain the electronic structure and electronic properties of the compound (*vide infra*).

Absorption Spectroscopic Study and Al^{3+} Sensing

The ligand, HL exhibits well-defined absorption bands at 450, 370, 317 and 267 nm in MeOH-H_2O (1:5,v/v) (HEPES buffer, pH = 7.4). Aqueous solution of different metal ions (Na^+, K^+, Ca^{2+}, Mg^{2+}, Ba^{2+}, Hg^{2+}, Ni^{2+}, Co^{2+}, Pb^{2+}, Pd^{2+}, Mn^{2+}, Cd^{2+}, Cu^{2+}, Fe^{3+}, Fe^{2+} and Zn^{2+}) has been added to methanol solution of HL maintained at pH, 7.4 and the absorption spectra are recorded. The spectral pattern of HL does not show any significant change on adding majority of metal ions except Al^{3+} (**Fig. 3**). The interaction of HL with Al^{3+} has been examined by

spectrophotometric titration at 25°C in MeOH-water (1:5, v/v, pH=7.4) (**Fig. 3)** . Intense absorption of HL at 450 nm has been blue shifted to 360 nm upon addition of Al^{3+} solution and naked eye observation is the changes of colour from bright yellow to colorless. The bright yellow color has remained unchanged in presence of other metal ions (**Supplementary material, Fig. S8**). The spectral observation undoubtedly suggests the conversion of free HL to the corresponding Al^{3+} complex. The appearance of isosbestic point (298 nm) also clearly indicates that the reaction is clean and straightforward. The change of absorbance is linear until the molar ratio [Al^{3+}] : [HL] reaches 1 : 1, and no longer changes with increase in [Al^{3+}]. It suggests that the stoichiometry between HL and Al^{3+} is 1 : 1 and the association constant (K_a) is 1.38(1) x 10^4 M^{-1} L (**Supplementary Material, Fig. S9)**. Preference of HL to Al^{3+} has been examined by solution absorption spectral presentation by adding O-donor ligands such as Na_2EDTA, citrate, oxalate, acetate to the solution. The spectral pattern and symmetry remains undisturbed only the absorption intensity of L-Al^{2+} is increased slightly upon addition of O-donor ligands in the ratio Al^{3+} : HL : O-donor ligands 1:1:1 **(Supplementary Materials, Fig. S12).** However, increase concentration of O-donor ligands even upto 1:1:6 does not show any change. This implies higher preference of HL to Al^{3+}.

Fluorescence spectroscopic study

The ligand, HL, emits weakly at 520 nm when excited at 370 nm and the fluorescence quantum yield is (ϕ_{HL}) 0.0057. The excitation at 450 nm does not show any emission while excitation of other absorption bands at 317 and 267 nm also show emission at 520 nm. On gradual addition of Al^{3+} the emission band of HL (520 nm) is blue shifted to 425 nm. The fluorescence spectrum of HL with other cations (Na^+, K^+, Ca^{2+}, Mg^{2+}, Ba^{2+}, Hg^{2+}, Ni^{2+}, Co^{2+}, Pb^{2+}, Pd^{2+}, Mn^{2+}, Cd^{2+}, Cu^{2+}, Fe^{3+} and Zn^{2+}) using their acetate salts in MeOH–water (1:5, v/v, pH=7.4) solution have been

examined on excitation at 370 nm (**Fig. 4**) and the turn-on emission is observed in presence of Al^{3+} at room temperature (25°C). On increasing [Al^{3+}] to the solution of HL the fluorescence intensity increases and becomes saturated when reached at 1:1 molar ratio which results enhancement of quantum yield (ϕ, 0.137, 24 fold compared to ligand) (**Fig. 4**). Addition of excess of [Al^{3+}] has no effect on the emission intensity of the mixture. Such an enhancement in fluorescence intensity is very selective for Al^{3+} (**Fig. 5**). The increment in fluorescence intensity for HL+Al^{3+} may arise from the elimination of photoinduced electron transfer (PET) in free HL and chelation enhancement effect (CHEF) through the co-ordination of azomethine-N and phenolic-O to metal ion (**Scheme 1**). To get further insight about the complexation reaction of HL and Al^{3+} fluoremetric titration has been done in MeOH-H_2O (1:5,v/v, pH =7.4) (**Fig. 6c**). [(F_{max}-F_0) / (F-F_0)] vs 1/[Al^{3+}] has been plotted following Benesi-Hildebrand equation (**Fig. 6b**) and a straight line is obtained. From the slope of the best fit line binding constant [K_d, (1.04 ± 0.01) x10^4] has been calculated. The limit of detection (LOD) of Al^{3+} has been calculated 33.2 nM following the 3σ method (**Supplementary Material, Fig. S10**)**.** The fluorescence enhancement of L-Al^{2+} complex has been persisted in existence of other metal ions. Hence, HL can detect Al^{3+} selectively in biological or environmental samples even in presence of other metal ions. Naphthyl appended fluorophores are efficient detector of Al^{3+} at very low concentration level. Singh *et al* [57] reported lowest LOD of Al^{3+} (1.35 nM) using (E)-*N*-[(2-hydroxy-naphthalen-1-yl)methylene]thiophene-2-carbohydrazide and second lowest LOD was obtained by Das *et al* [58] (10 nM) with 2-((naphthalen-6-yl)methylthio)ethanol. In this work we report third lowest LOD of Al^{3+} (33.2 nM). Other reports show LOD of Al^{3+} higher than 50 nM [18]. Although present report is in third position in the detection efficiency series but its advantage is the use of biocompatible sulfonamide derivative. Sulfonamides are established drug; hence

they are biofriendly and nontoxic (see below MTT assay, ADMET test). Effect of pH variation on fluorescence intensity of HL and L-Al^{2+} complex has been studied; it has observed that there is no significant fluorescence emission of HL at the pH range of 4 to 12 but in presence of Al^{3+} the ligand emits in the pH range between 4.0 to 8.5 (**Fig. 7**). This finding indicates that HL is useful for detection of Al^{3+} in biological pH. To establish the binding stoichiometry of HL and Al^{3+} Job's Plot has been generated by plotting fluorescence intensity against different mole fractions of Al^{3+} while volume of solution has remained fixed (**Supplementary Material, Fig. S11**). Maxima in this plot has been obtained at ~0.5 mole fraction, which suggests about 1:1 complex formation of HL and Al^{3+}. Upon addition of one equivalent of O-donor ligands such as Na_2EDTA, citrate, oxalate, acetate to the solution of L-Al^{2+} the fluorescence intensity is decreased by 20% (Na_2EDTA), 36% (oxalate, acetate) and 44% (citrate); however, complete recovery of HL has not been successful even in presence of large excess (>10 times) of O-donor ligands (**Supplementary Material, Fig. S13).** This is supportive to absorption spectroscopic data of preference of HL to Al^{3+}.

Time resolved flourescence measurement of HL in presence and absence of Al^{3+} shows that complexation enhances life time ($\tau_{complex}$, 0.9 ns) than the free ligand (τ_{HL} , 0.05 ns). The decay profile of HL and of its L-Al^{2+} complex is shown in **Fig. 8**. Lifetime data were taken on excitation at 370 nm. The fluorescence decay fits bi-exponential nature. The radiative and non-radiative rate constants (kr and knr) were calculated and the data show knr values, which are unusually higher with respect to the kr ones (**Supplementary Material, Table S2**).

Stoichiometric study by NMR Titration

To elucidate the nature of the binding of HL to Al^{3+} the ^1H NMR spectrum of HL has been investigated in absence and in presence of Al^{3+} in CD_3OD (**Fig. 9**). The ^1H NMR spectrum of HL shows signals for HC=N (azomethine) at 9.64 ppm and other aromatic-Hs appear at 6.97 to 8.32 ppm (**Supplementary Material, Fig. S3**) and in Al-L^{2+} complex the naphtholato-Hs (3-H to 8-H; $\Delta\delta$ = 0.053 (3-H), 0.015 (4-H), 0.158 (5-H), 0.108 (6-H), 0.035 (7-H), 0.351 (8-H) ppm respectively)), imine-H (11-H, $\Delta\delta$ = 0.41 ppm) undergo downfield shifting while aromatic/heterocyclic ring(s) of sulfonamide,13-H to 19-H shift to lower δ ($\Delta\delta$ = 0.369 for 14, 16-H ppm; 0.777 ppm for 13, 17-H; 0.166 ppm for 19-H). Addition of 0.5 equivalents of $Al(NO_3)_3$ leads to a downfield shift of the signal corresponding to the CH=N proton ($\Delta\delta$ = 0.506 ppm) (**Fig. 9**). The co-ordination through phenolic oxygen atoms confirmed by NMR titration as the signal of phenolic-OH signal (δ, 11.46 ppm) is vanished after addition of one equivalent $Al(NO_3)_3$. Thus, according to the ^1H NMR titration data, interaction of HL with Al^{3+} leads to the formation of a $[Al\text{-}L]^{2+}$ structure. The stoichiometry of L-Al^{2+} complex has been further established by means of mass spectroscopic data. ESI-MS data of HL and Al-L^{2+} gives a peak at m/z 408.13 and 486.17 (**Supplementary Material, Figs. S1 and S5**) respectively which corresponds to $[Al(L)(OH)(H_2O)_2]^+$ and signifies the 1:1 complexation.

Density Functional Theory Calculation

Geometry optimization of HL and $[Al(L)(OH)(H_2O)_2]^+$ has been performed using DFT calculation with B3LYP method and 6-31G(d,p) basis set. Based on mass spectral data composition of the complex ion has been assigned as $[Al(L)(OH)(H_2O)_2]^+$. According to DFT optimized structure Al is penta-coordinated and distorted square pyramid in geometry (**Fig. 10**). HL acts as mono anionic N, O chelator to Al^{3+}; theoretically calculated Al-N(imine) and Al-O(phenolato) distances are 1.946 Å and 1.827 Å, respectively and have been comparable with

similar structure [59,60]. Due to complex formation the C(8)-N(3), C(11)-N(3), C(13)-O(4) bond distances have been significantly elongated compared to free ligand (**Supplementary Material, Tables S3, S4**). The result shows that electron density in HOMO of HL is mainly distributed on the naphthyl ring and LUMO is distributed between naphthyl and sulfonamide moiety. For HOMO of $[Al(L)(OH)(H_2O)_2]^+$, the π electron density is allocated mainly on naphthyl ring but the LUMO is spread over azomethine, sulfonamide and naphthyl moiety. Contour plots of the selected orbitals of the compounds have been given in **Supplementary Material, Fig. S14** and **Fig. S15.** The HOMO-LUMO gap in HL (3.43 eV) has slightly increased in $[Al(L)(OH)(H_2O)_2]^+$ (3.64 eV) which supports the blue shift in UV-Vis spectra (**Fig.11**).

To interpret electronic spectra of HL and $[Al(L)(OH)(H_2O)_2]^+$ the TD-DFT calculation has been executed by DFT/B3LYP method using 6-31G(d, p) basis set in MeOH. The ligand exhibit four electronic transitions corresponding to 450, 370, 317, 267 nm and they are assigned for $S_0 \rightarrow S_1$, $S_0 \rightarrow S_3$, $S_0 \rightarrow S_{11}$, $S_0 \rightarrow S_{20}$ (**Fig. 12**). In the UV-Vis spectra of HL there is a strong band at visible region (450 nm) which is assigned to HOMO → LUMO, intramolecular charge transfer π(naphthyl ring)→ π*(naphthyl/ sulphonamide ring), and it is blue shifted upon addition of Al^{3+} giving rise to 360 nm (**Fig. 14**). The complex shows three bands at 360, 318 and 267 nm in UV-Vis spectrum (**Fig. 3**) who are assigned to $S_0 \rightarrow S_1$, $S_1 \rightarrow S_4$ and $S_0 \rightarrow S_{11}$ transitions (**Fig. 13**). Absorption energies of HL and its Al^{3+} complex along with their oscillator strength are given in **Supplementary Material, Table S5**.

Biological application

Cell imaging

The application of HL as fluorescent probe for *in vitro* living cell imaging and detection of intracellular Al^{3+} ions have been studied on African green monkey kidney cells (Vero cells, ATCC, Manassas, VA, USA) using fluorescence microscope. The fluorescence imaging of intracellular Al^{3+} in living cells is shown in **Fig.14**. Vero cells fixed in paraformaldehyde (4%) and blocked with BSA in PBS-triton X100 solution. Then, the cells were observed under epifluorescence microscope.[48] Then, the cells were treated with Al^{3+} solution (10 μM HL+ 10 μM Al^{3+}) for 30 min in buffer for incubation, washed again with buffer at pH 7.4 and mounted on a grease free glass slide. Cells were observed under a fluorescence microscope equipped with a UV filter after adding HL (2 mM). Cells incubated only with Al^{3+} were used as a control. HL can permeate easily through tested living cells without any harm (as the cells remain alive even after 30 min of exposure to HL at 2 mM). The MTT assay has been applied for labeling dead cells to evaluate cytotoxicity of the probe and is shown in **Fig. 15**. The study shows that HL has no cytotoxicity towards cells upto 100 μg/ml (approx 250 μM)). These results indicate that the probe has a huge potential in both *in vitro* and *in vivo* applications as Al^{3+} sensor and in live cell imaging. ADMET (absorption, distribution, metabolism, excretion and toxicity) prediction of HL (**Supplementary Material, Table S6**) says that HL has good aqueous solubility and absorption, so it might have chemical activity for detection of Al^{3+} within living cells. These results in contrast to two other ligands of lower LOD[57,58]; the ligand, (E)-*N*-[(2-hydroxy-naphthalen-1-yl)methylene]thiophene-2-carbohydrazide shows LOD to Al^{3+} 1.35 nM but no cell imaging or cytotoxicity studies are reported. Although 2-((naphthalen-6-yl)methylthio)ethanol (LOD to Al^{3+}, 10 nM) [58] shows cell signaling activity but no cytotoxicity studies is reported. We have checked the mutagenic activity by using ADMET filtration and it is computed that 2-((naphthalen-6-

yl)methylthio)ethanol is mutagenic. Although present report of HL shows one order lower LOD to Al^{3+} but biologically more friendly and nonmutagenic.

Antibacterial and molecular docking studies

The fluorescent probe HL is a Schiff base derivative of sulfamethoxazole, so antimicrobial activity of HL against several Gram-positive (*S. aureus* ATCC21737, *Enterococcus facelis* ATCC 29212) and Gram-negative (*E. coli*, ATCC 25922, *S. typhi* MTCC734, *K. pneumonia* ATCC 714) bacterial strain. The Schiff base has shown moderate antimicrobial activity (MIC 32-64 μg/ml) (**Supplementary Material, Table S7**).

The molecular docking of HL has been carried out with DHPS (dihydropteroate synthase) to find the probable mode of binding using CDOCKER module of Receptor-Ligand Interaction section of Discovery Studio Client 4.1. It has been observed that there are 15 amino acid residues (Asn22, Ser27, Phe28, Ser61, Thr62, Arg63, Pro64, Asp96, Gln149, Gly189, Phe190, Lys221, Ser222, Gln226, Arg255) (**Fig. 16**) close to the ligand in DHPS-HL complex and HL forms three H-bonds with Ser61 (2.51 Å, ∠D-H-A (Ser OH...N oxalyl) 160º), Arg63 (2.93 Å, ∠D-H-A (Arg NH...N oxalyl) 116º) and Ser222 (2.83 Å, ∠D-H-A (Ser HO....HO phenol) 103) (**Fig. 17, 18**). In the best docked pose of L the binding energy ($E_{Binding}$= Ec_{omplex} - E_{ligand}- $E_{receptor}$) is -53.7Kcal/mol (**Supplementary Material, Table S8**).

Conclusion

In summary, naphthyl attached to sulfonamide by –C=N- has been successfully prepared and serves as selective fluorogenic probe to Al^{3+} ion in presence of large number of other metal ions.

The receptor itself is weakly fluorescent while Al^{3+} has enhanced its emission by 24 fold and limit-of-detection (LOD), 33.2 nM, is third lowest in the series of naphthyl based sensor. The binding composition of receptor and Al^{3+} is 1:1 and that has been established by ^1H NMR, MS studies and further supported by DFT computation. Cell imaging experiment and MTT assay reveals that the new ligand can be efficient probe to detect Al^{3+} in the biological samples. The advantage of present sensor over other reported molecules[57,58] are [a] least interference by other metal ions, [b] experiment requires less organic solvents, [c] it is non mutagenic, less toxic and compatible in biological pH, [d] it is the 1st reported molecule from sulfonamide family to detect Al^{3+} cation. Besides, sulfonamide Schiff base antibacterial activity against several Gram-positive (*S. Aureus* ATCC21737, *Enterococcus facelis* ATCC 29212) and Gram-negative (*E. coli*, ATCC 25922, *S.Typhi* MTCC734, *K. pneumonia* ATCC 714 bacterial strain of MIC, 32-64 μg/ml.

Supplementary materials

Reaction detail in **Scheme S1**; The spectral data of HL (Mass, **Fig. S1**; FT-IR, **Fig. S2**; ^1H NMR, **Fig. S3;** ^{13}C NMR, **Fig. S4.**), MS spectrum of $[L\text{-}Al(OH)(H_2O)_2]^+$ **(Fig. S5**); IR spectrum of $[L\text{-}Al(OH)(H_2O)_2]^+$ **(Fig. S6);** ^1H NMR spectrum of the complex (**Fig. S7);** naked eye observation of colour change of HL solution by adding different cation (**Fig**. **S8**); Benesi-Hildebrand plots (**Fig. S9**), Limit of detection (LOD), (**Fig. S10**); Job's plot (**Fig. S11);** effect of O-donor chelating agents on absorption spectrum of $L\text{-}Al^{2+}$ (**Fig**. **S12**); effect of O-donor chelating agents on fluorescence spectrum of $L\text{-}Al^{2+}$ (**Fig**. **S13**); contour plots of HL(**Fig. S14**); contour plots of $[L\text{-}Al(OH)(H_2O)_2]^+$ **(Fig. S15**). Hydrogen Bonds for HL (**Table S1**); Life time data of L and $L\text{-}Al^{2+}$ complex (**Table S2);** Selected geometrical parameter (calculated) of $L\text{-}Al^{2+}$ in the ground state (**Table S3**); Change in bond length (calculated) in ($Al\text{-}L^{2+}$) compared to free ligand (HL) (**Table S4**); Calculated transitions and their assignment for ligand (HL) and Al^{3+}-complex

(**Table S5);** ADMET prediction data (**Table S6**); Antimicrobial results (MIC) of HL (**Table S7);** Docking score of HL with DHPS protein (downloaded from PDB) (**Table S8**);

Crystallographic data for the structure have been deposited to the Cambridge Crystallographic Data center, CCDC No. 1405369 for HL.These data can be obtained free of charge via http://www.ccdc.cam.ac.uk/conts/retrieving.html, or from the Cambridge Crystallographic Data Centre, 12 Union Road, Cambridge CB2 1EZ, UK; fax: (+44) 1223-336-033; or e-mail: deposit@ccdc.cam.ac.uk.

Acknowledgement

Financial support from West Bengal DST (228/1(10)/(Sanc.)/ST/P/S&T/9G-16/2012), Kolkata and University Grants Commission (F.42-333/2013(SR)), New Delhi are gratefully acknowledged. S. Mondal is thankful to UGC, New Delhi, India for fellowship. We are thankful to Mr. Kumer Saurav Keshri an M.Sc student of Indian School of Mines, Dhanbad, for his initial contribution in the synthesis and some characterisation part of this work.

References

1. P. Nayak, *Environ. Res.*, 2002, **89**, 101-115.

2.(a) T. P. Flaten, *Brain Res. Bull.,* 2001, **55**, 187-196; (b) J. R. Walton, *Curr. Inorg. Chem.,* 2012, **2**, 19-39.

3. J. R. Walton, *NeuroToxicology.,* 2006, **27**, 385-394.

4. R. W. Gensemer, R. C. Playle, *Crit. Rev. Environ. Sci. Technol*., 1999, **29**, 315-450.

5. C. M. Gergichevich, M. Alberdi, A.G. Ivanov , M. Reyes-Díaz, *J. Plant Nutr. Soil Sci*., 2010, **10**, 217-243.

6. M.L. Mora, M.A. Alfaro, S.C. Jarvis, R. Demanet , P. Cartes, *Soil Use Manag*., 2006, **22**, 95-101.

7. T. Han, X. Feng, B. Tong, J. Shi, L. Chen, J. Zhic , Y. Dong, *Chem. Commun.,* 2012, **48**, 416-418.

8. A. Dhara, A. Jana, N. Guchhait, P. Ghosh, S. K. Kar, *New J. Chem.,* 2014, **38**,1627-1634.

9. S. Kim, J.Y. Noh, S.J. Park, Y.J. Na, I.H. Hwang, J.Min, C.Kim, J. Kim, *RSC Adv.,* 2014, **4**, 18094-18099.

10. A. Zioła-Frankowska, M. Frankowski, J. Siepak, *J. Talanta.,* 2009, ***79***, 623-630.

11. F. Zheng, B. Hu, *Spectrochim. Acta, Part B* , 2008, **63**, 9-18.

12. F. Thomas, A. Maslon, J.Y. Bottero, J. Rouiller, F. Montlgny, F. Genevrlere, *Environ. Sci. Technol.,* 1993, **27**, 2511-2516.

13. Y.H.Ma, R.Yuan, Y.Q.Chai, X.L.Liu, *Mater. Sci. En.,* 2010, **30**, 209-213.

14. M. Bolte, Y. Garcia, D. Das, *Dalton Trans*., 2013, **42**, 13311–13314.

15. S. Das, A.Sahana, A. Banerjee, S. Lohar, D. A. Safin, M. G. Babashkina, M. Bolte, Y. Garcia, I. Hauli, S. K. Mukhopadhyay, D. Das, *Dalton Trans*., 2013, **42**, 4757–4763.

16. J. R. Walton, *Curr. Inorg. Chem*., 2012, **2**, 19-39.

17. L. Wang, W. Qin, X. Tang, W. Dou, W. Liu, Q.Teng, and X. Yao, *Org. Biomol. Chem.*, 2010, **8**, 3751–3757.

18. D. Karak, S. Lohar, A. Banerjee, A. Sahana, I. Hauli, S. K. Mukhopadhyay, J. S. Matalobos, D. Das, *RSC Advances*, 2012, **2**, 12447–12454.

19. S. Goswami, K. Aich, S. Das, A. K. Das, D. Sarkar, S. Panja, T. K. Mondal, S. Mukhopadhyay, *Chem. Commun.,* 2013, **49**, 10739--10741.

20. A.Sahana ,A. Banerjee, S.Lohar, B.Sarkar, S. K.Mukhopadhyay, D. Das, *Inorg. Chem*. 2013, **52**, 3627−3633.

21. A. Sahana, A. Banerjee, S. Lohar, A. Banik, S. K. Mukhopadhyay, D. A. Safin, M. G. Babashkina, M. Bolte, Y. Garcia, D. Das, *Dalton Trans.,* 2013, **42**, 13311–13314.

22. H.Shengli, S. Jingjing, W.Gongying, C. Cuixia, G. Qing, *Spectrochim Acta A*., 2015, **136**, 1188-1194.

23. T. Ma, M. Dong, Y. Dong, Y. Wang, Y. Peng, *Chem. Eur. J.,* 2010, **16**, 10313 – 10318

24. B. Sen, M. Mukherjee, S. Banerjee, S. Palaand , P. Chattopadhyay, *Dalton Trans*., 2015, **44**, 8708–8717.

25. Y. Mi, D. Liang, Y. Chen, X. Luo , J. Xiang *RSC Adv.,*2014, **4**, 42337-42345.

26. S. Lee, G. You, Y. Choi, H. Jo, A. R. Kim, I. Noh, S. J. Kim, Y. Kim , C. Kim, *Dalton Trans***.**, 2014, **43**, 6650-6659.

27. C. H. Chen, D.J. Liao, C. F. Wan, A.T. Wu, *Analyst***.**, 2013, **138**, 2527-2530.

28. J. Kumar, M. J. Sarma, P. Phukan , D. K. Das, *Dalton Trans*., 2015, **44**, 4576-4581.

29. M.V. Lopez, M. R. Bermejo, M. E. Vazquez, A. Taglietti, G. Zaragoza, R. Pedrido, M. Martınez-Calvo, *Org. Biomol. Chem.*. 2010**, 8***,*** 357–362.

30. J. Li, H. Chen, H. Lin, H.K. Lin, *J. Photochem. Photobiol. B*., 2009**, 97***,*** 18–21.

31. X-F.Shang, H. Lin, H.K. Lin, *J. Fluorine Chem,*. 2007**, 128***,*** 530–534.

32. S.V. Bhosale, M.B. Kalyankar, S. Langford, J. *Org. Lett.,* 2009**, 11***,*** 5418–5421.

33. L.N. Ferguson. *Chem. Rev.,* 1946, **38,** 227-254.

34. B. Valuer, Molecular Fluorescence: Principles and Applications, Wiley-VCH, Weinheim, 2001.

35. R. H. Blessing, *Acta Cryst. A*., 1995, **51**, 33–38.

36. G. M. Sheldrick, *Acta Cryst A.,* 2008, **64**, 112-122.

37. L.J. Farrugia, *J. Appl. Cryst.,* 1997, **30**, 565-565.

38. L. J. Farrugia, WinGX, *J. Appl. Cryst.,* 1999, **32**, 837–838.

39. A.D. Becke, *J. Chem. Phys.,* 1993, **98**, 5648-5652.

40. M . JFrisch, G.W. Trucks, H.B. Schlegel, G.E. Scuseria, M.A. Robb, J.R. Cheeseman, G. Scalmani, V. Barone, B. Mennucci, G.A. Petersson, H. Nakatsuji, M. Caricato, X. Li, H.P. Hratchian, A.F. Izmaylov, J. Bloino, G. Zheng, J.L. Sonnenberg, M. Hada, M. Ehara, K. Toyota, R. Fukuda, J. Hasegawa, M. Ishida, T. Nakajima, Y. Honda, O. Kitao,

H. Nakai, T. Vreven, Jr.J.A. Montgomery, J.E. Peralta, F. M. Ogliaro, J. Bearpark, J. Heyd, E. Brothers, K.N. Kudin, V.N. Staroverov, R. Kobayashi, J. Normand, K. Raghavachari, A. Rendell, J.C. Burant, S.S. Iyengar, J. Tomasi, M. Cossi, N. Rega, J.M. Millam, M. Klene, O.Yazyev, A.J. Austin, R. Cammi, C. Pomelli, J.W.Ochterski, R.L.Martin, K. Morokuma, V. G. Zakrzewski, G.A.P.; Salvador, J.J. Dannenberg, S. Dapprich, A.D. Daniels, Ö. Farkas, J.B. Foresman, J.V. Ortiz, J. Cioslowski, D.J. Fox, Gaussian, Inc., CT Wallingford, 2009**.**

41. R. Bauernschmitt, R. Ahlrichs, *Chem. Phys. Lett.,* 1996, **256** , 454-464.

42. R.E. Stratmann, G.E. Scuseria, M.J. Frisch, *J. Chem. Phys.*, 1998, **109** , 8218.

43. M.E. Casida, C. Jamorski, K.C. Casida, D.R. Salahub, *J. Chem. Phys.,* 1998, 108, 4439-4449.

44. V. Barone, M. Cossi, *J. Phys. Chem. A.,* 1998, **102** , 1995 - 2001.

45. M. Cossi, V. Barone, *J. Chem. Phys.,* 2001, **115**, 4708 -4717.

46. M. Cossi, N. Rega, G. Scalmani, V. Barone, *J. Comput. Chem.,* 2003, **24** , 669 -681.

47. N. M. O'Boyle, A. L. Tenderholt, K. M. Langner,. *J. Comput. Chem.,* 2008, **29**, 839-845.

48. P. Bag, D. Ojha, H. Mukherjee, U.C. Halder, S. Mondal, N.S. Chandra, S. Nandi, A. Sharon, M. Sarkar Chawla, S. Chakrabarti, and D. Chattopadhyay, *PLoS One*, **2013**, 8(10) e77937.

49. D. Banerjee, S.M. Mandal, A. Das, M.L. Hegde, K.K. Bhakat, *J. Biol.Chem.,* 2011, **286**

6006-6016

50. P. Bag, D. Ojha, H. Mukherjee, U.C. Halder, S. Mondal, A. Biswas, A. Sharon, K. Luc Van, S. Chakraborty, G. Das, D. Mitra, and D. Chattopadhyay. *Antiv. Res.,* 2014, **105**,126-134.

51. Twentieth Informational Supplement. CLSI document M100-S20-U. Wayne: CLSI; 2010.

52. T. Samanta, G. Roymahapatra, W. F. Porto, S. SethGhorai, S. Saha, J. Sengupta, O. L. Franco, J. Dinda, S. M. Mandal, *PLoS One,* 2013, **8**, 58346-583457.

53. D. Das, N. Sahu, S. Roy, P. Dutta, S. Mondal, E. L. Torres, C. Sinha, *Spectrochim. Acta A*, 2015, **137** , 560–568

54. E. S. Lang, L. L. Marques, G.M. de Oliveira, *Z. Naturforsch*., 2005, **60b** , 1264 – 1268.

55. K. K. Upadhyay , S. Upadhyay , A. Kumar , K. Thapliyal, *J. Sulfur Chem.,* 2012*,* **33** , 573-582.

56. S. Mondal, S. M. Mandal, T. K. Mondal, C. Sinha, *Spectrochim. Acta A*, 2015, **150**, 268–279.

57. K. Tiwari , M. Mishra, V.P. Singh, *RSC Adv.,* 2013, **3**, 12124–12132.

58. A.Banerjee, A. Sahana, S. Das, S. Lohar, S. Guha, B. Sarkar, S. K. Mukhopadhyay, A. K. Mukherjee, D. Das, *Analyst,* 2012, **137**, 2166-2175 .

59. E. S. Aazam and M. P. Coles, *Cent. Eur. J. Chem.* , 2010, **8**, 1305-1310

60. W. -L. Kong, Z. –Y. Chai and Z. –X. Wang, *Dalton Trans*., 2014, **43**, 14470–14480

Table 1. Crystallographic data of HL

Empirical formula	$C_{21}H_{17}N_3O_4S$
Formula weight	407.44
Temperature (K)	296(2)
system	Triclinic
Space group	P-1
a(Å)	8.3710(5)
b(Å)	10.0074(6)
c(Å)	12.8160(8)
α(Å)	67.264(4)
β (°)	80.722(5)
γ(°)	86.904(5)
V(Å)^3	977.20(10)
Z	2
μ (MoK$_\alpha$) (mm^{-1})	0.199
θ range	1.74-25.00
D_{calc} (mg m^{-3})	1.385
Refine parameters	0.067
Total reflections	13194
Unique reflections	3316
R_1[a] [I > 2σ (I)]	0.0602
wR_2[b]	0.1661
GOF[c]	0.989

[a]$R = \Sigma||F_o|-|F_c||/\Sigma|F_o|$; [b]$wR = \{\Sigma[w(F_o^2-F_c^2)^2]/\Sigma[w(F^2_o)^2]\}^{1/2}$; $w = [\sigma^2(F_o)^2 + (0.0805P)^2]^{-1}$

where $P = (F_o^2 + 2F_c^2)/3$; [c] Goodness-of-fit

Table 2 . Selected geometrical parameters of HL

	Bond distance(Å) X-ray	Calculated		Bond angle(°) X-ray	Calculated
C(8)-N(3)	1.402(4)	1.408	C(7)-C(8)-N(3)	117.3 (3)	117.45
C(11)-N(3)	1.327(4)	1.316	C(8)-N(3)-C(11)	126.86	122.91
C(11)-C(12)	1.383(5)	1.435	N(3)-C(11)-C(12)	123.3(4)	121.94
C(12)-C(13)	1.450(5)	1.420	C(11)-C(12)-C(13)	119.7(3)	118.92
C(13)-C(14)	1.407(5)	1.419	C(12)-C(13)-O(4)	120.8(4)	121.66
C(13)-O(4)	1.274(4)	1.352	C(14)-C(13)-O(4)	120.7(4)	108.32
O(4)-H(1)	0.899(2)	1.032	O(2)–S(1)–N(2)	105.16(18)	100.67

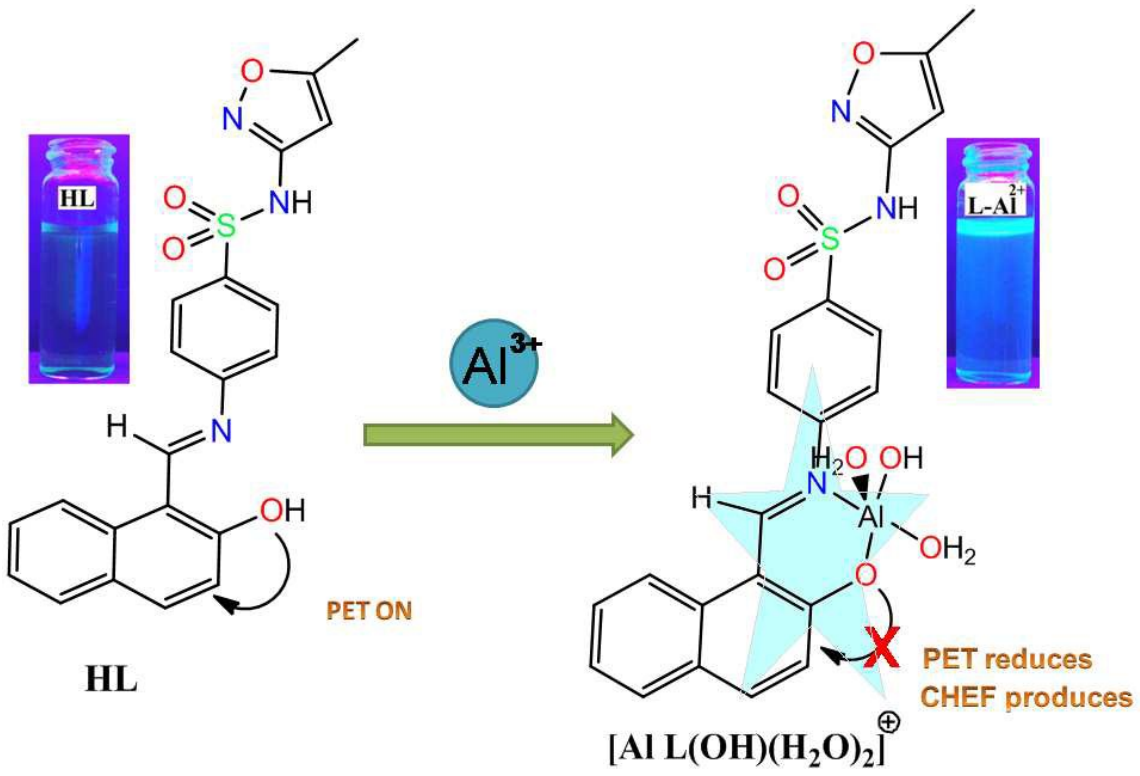

Scheme 1: Schematic representation of enhancement of fluorescence of HL in presence of Al^{3+}.

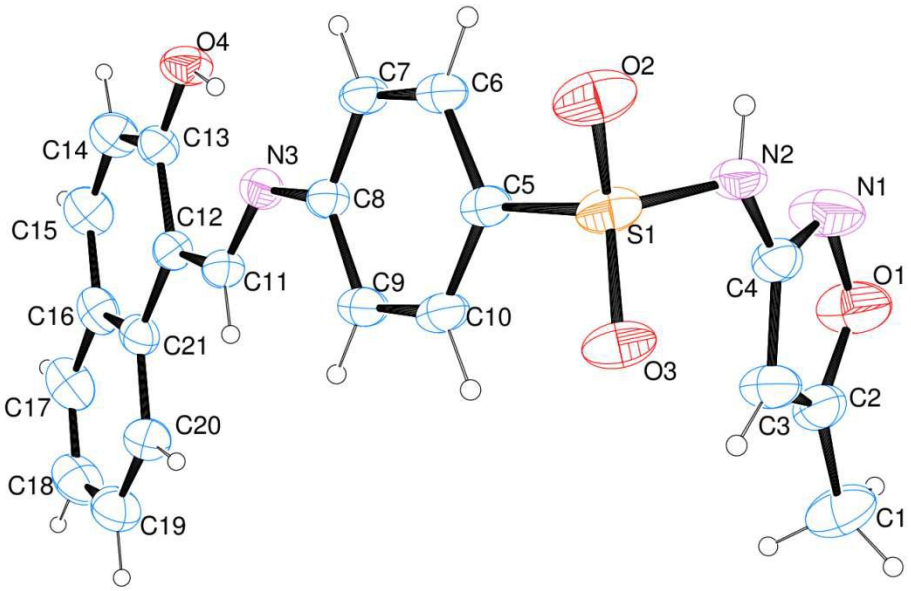

Fig. 1. ORTEP plot of HL with 35% ellipsoidal probability

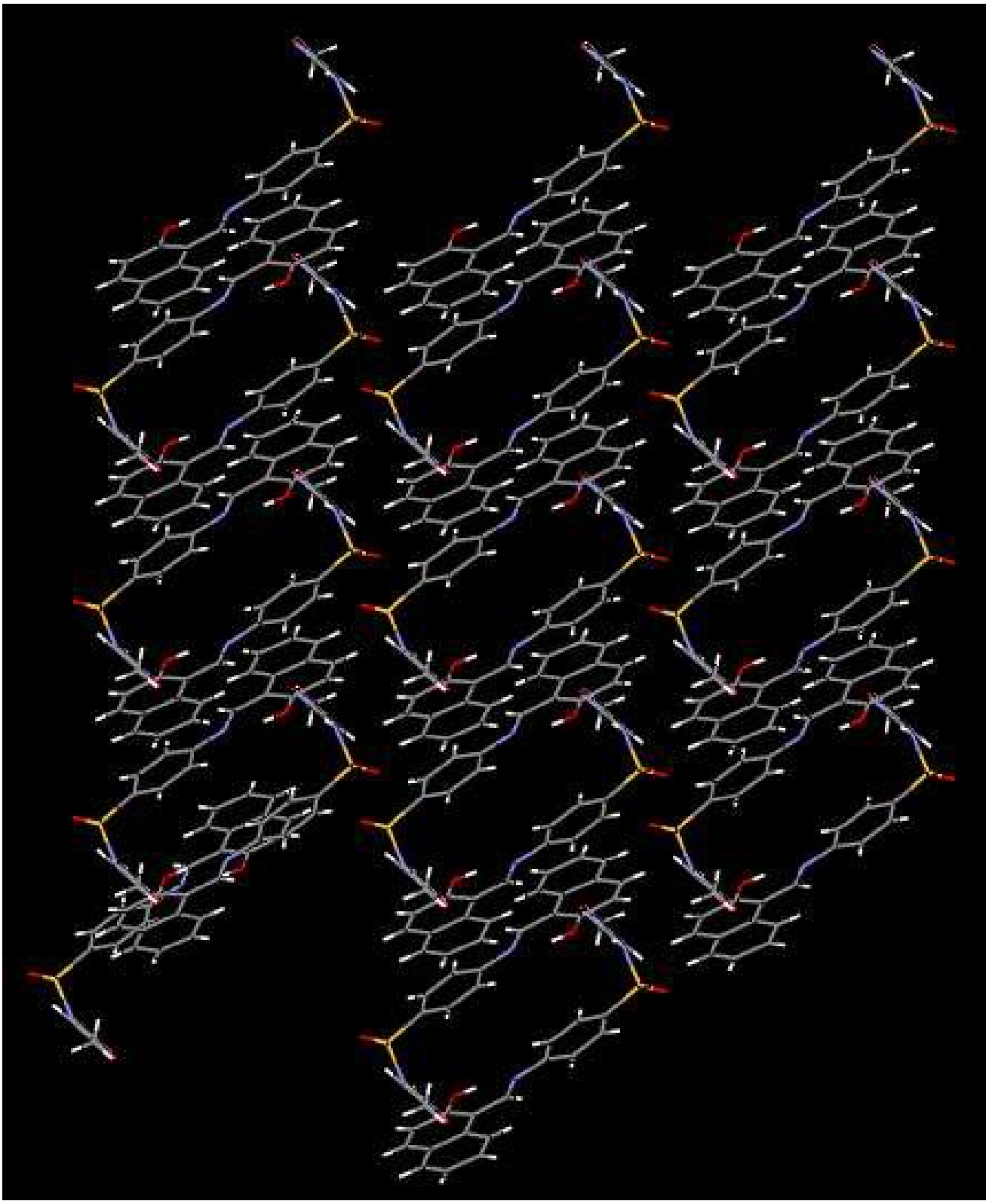

Fig.2. 2D supramolecular structure generated by hydrogen bonding and π---π interaction in HL

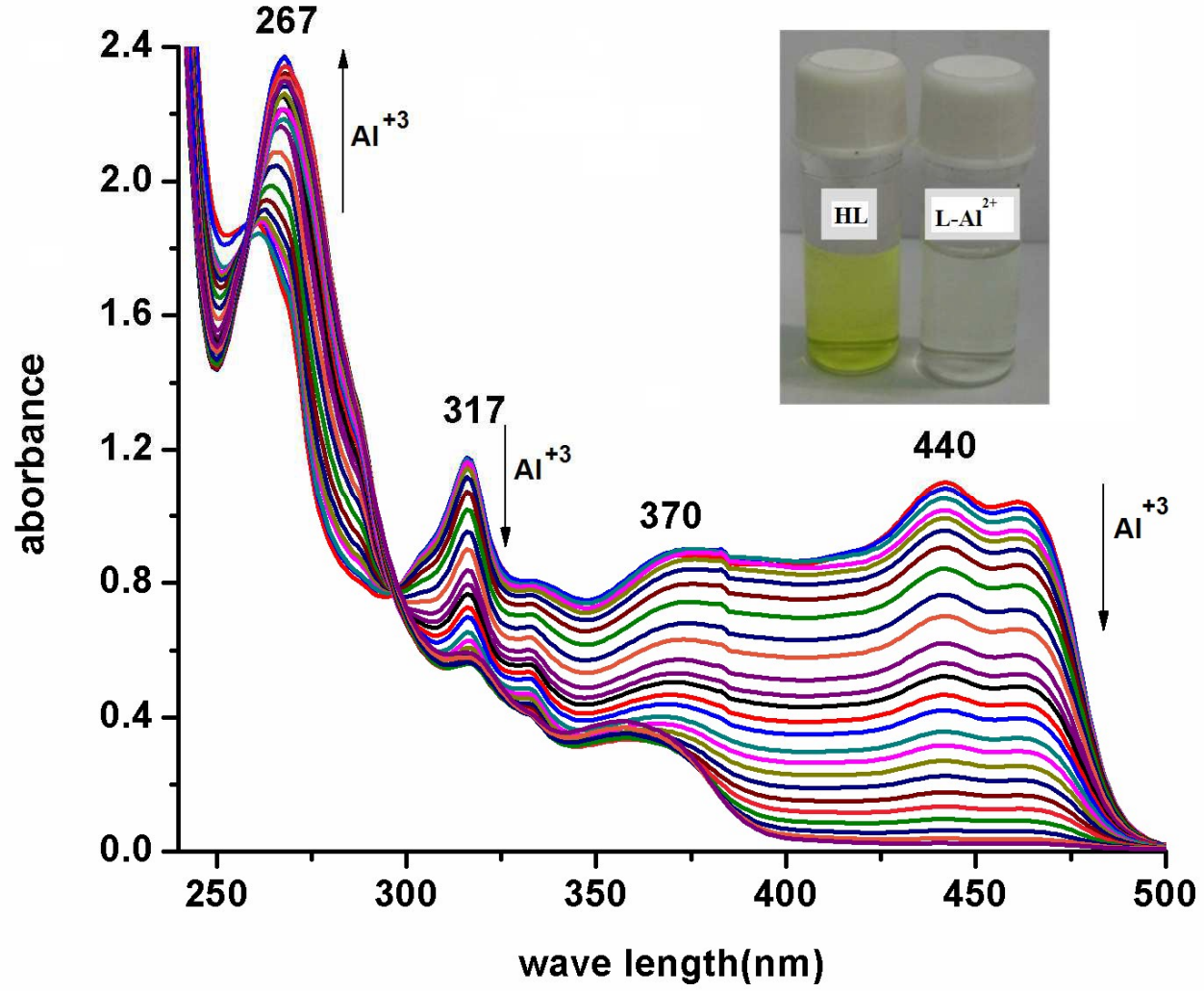

Fig.3. Change in absorption spectra of HL on gradual addition of Al^{3+}

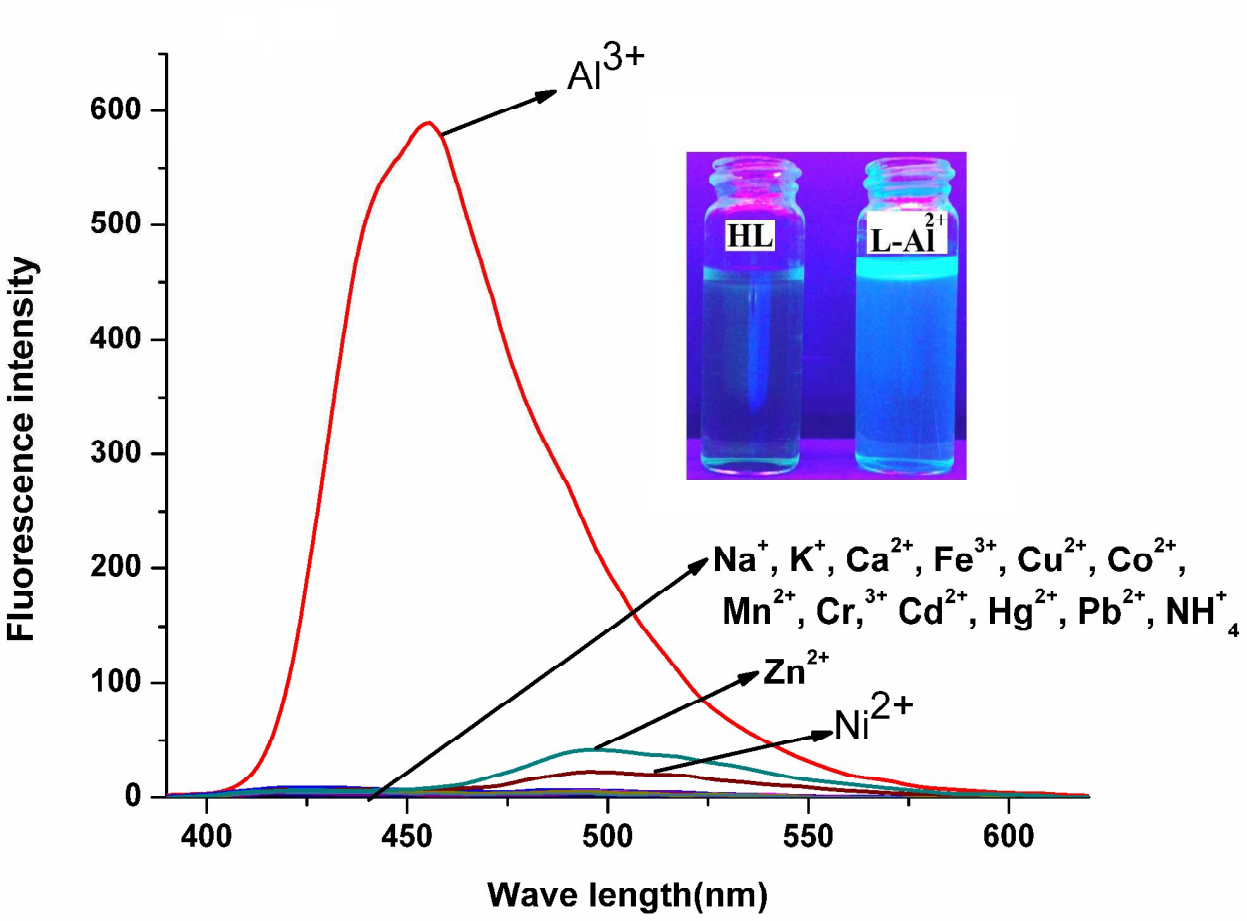

Fig.4. The receptor (HL) shows strong emission in presence of Al^{3+}at 450 mn on excitation at 360 nm.

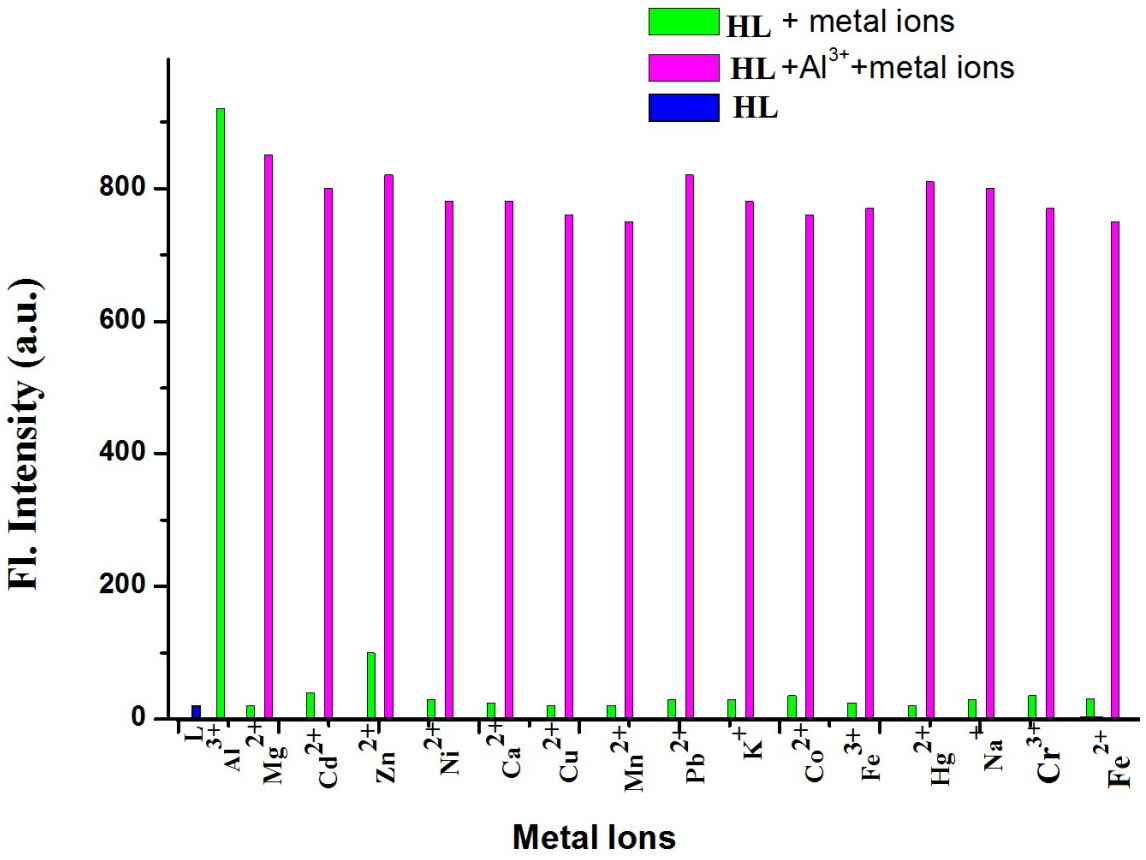

Fig.5. Bar chart presenting fluorescence response of HL in presence of different metal ions

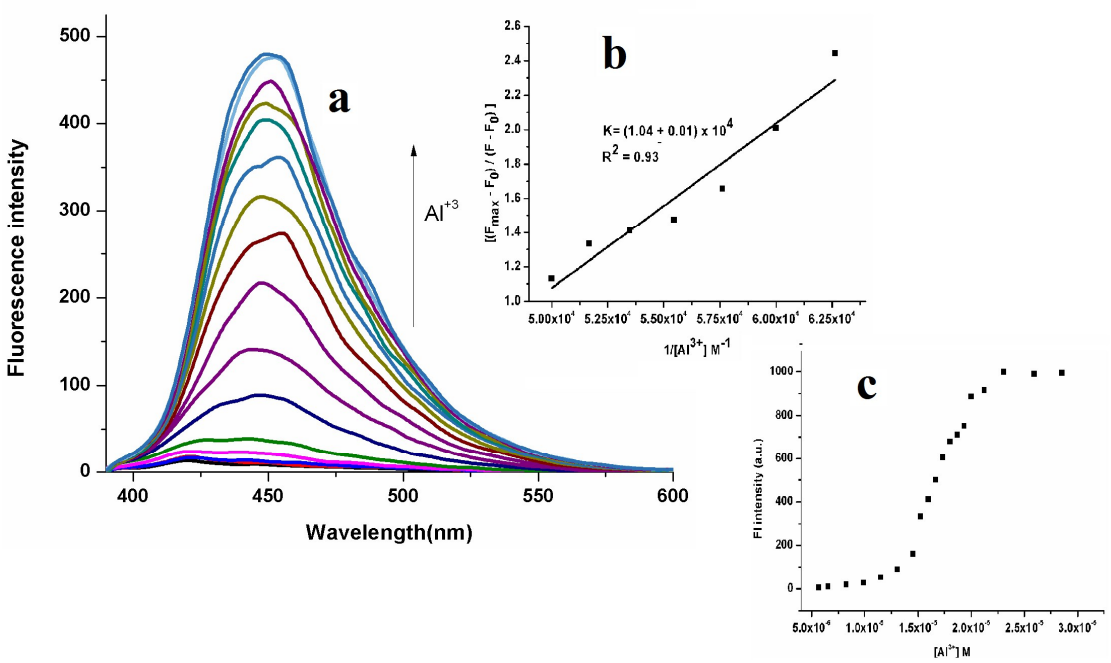

Fig.6. (a) Fluorescence titration of HL in MeOH-water (1:5, v/v, pH7.4) by the gradual addition of Al^{3+} with λ_{ex}= 370nm, (b) Benesi-Hilderman plot, and (c) plot of fluorescence intensity vs $[Al^{3+}]$

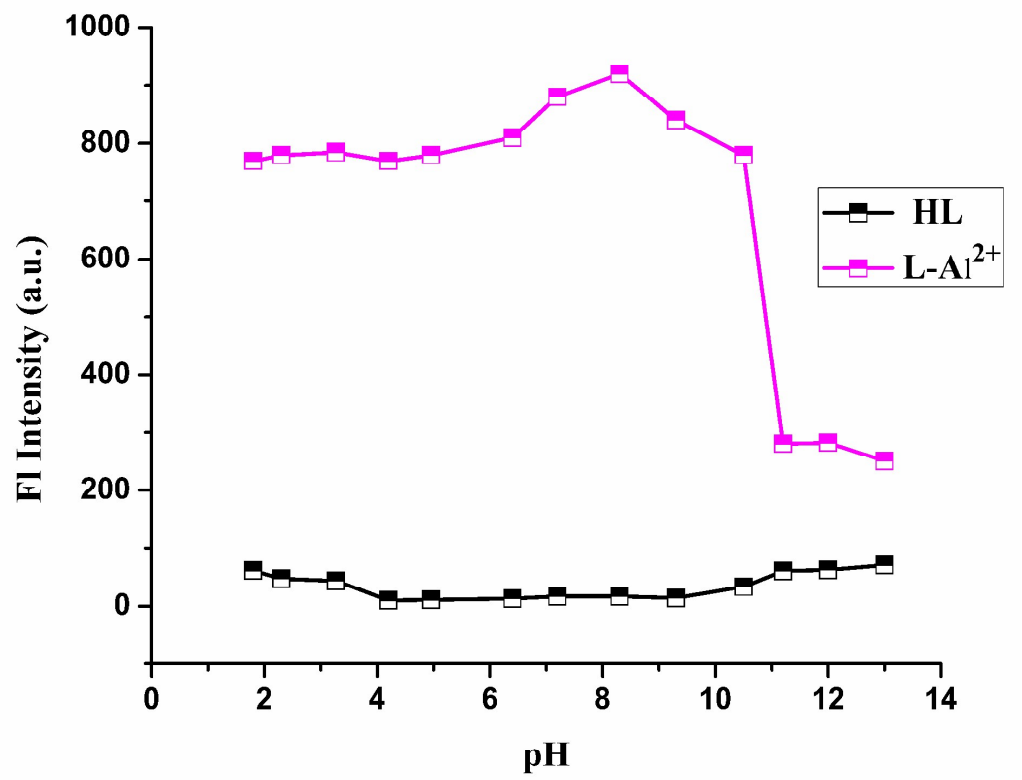

Fig.7. Fluorescence intensity of HL and L-Al^{2+} complex at different pH

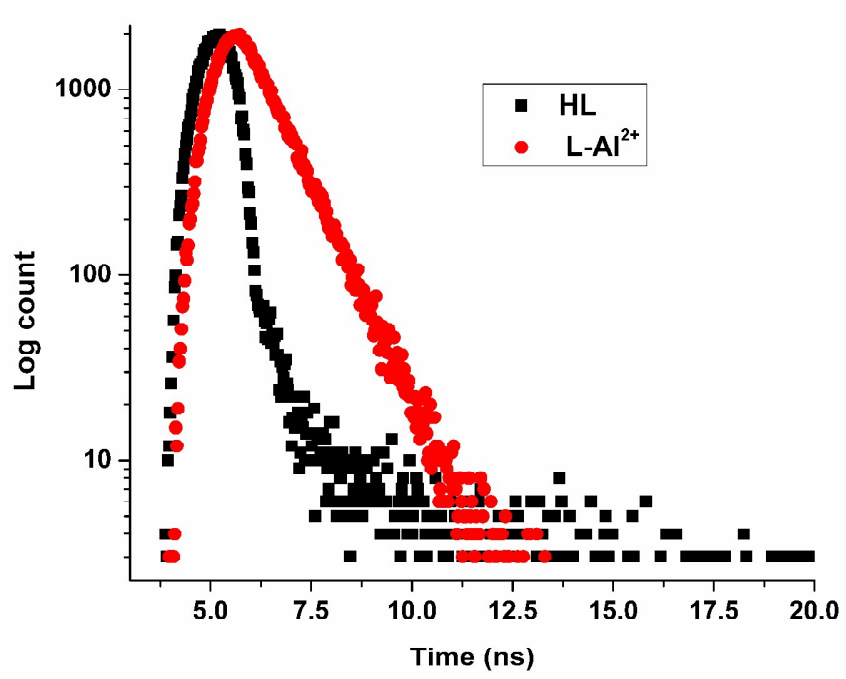

Fig.8. Decay profile of HL and L-Al^{2+} complex

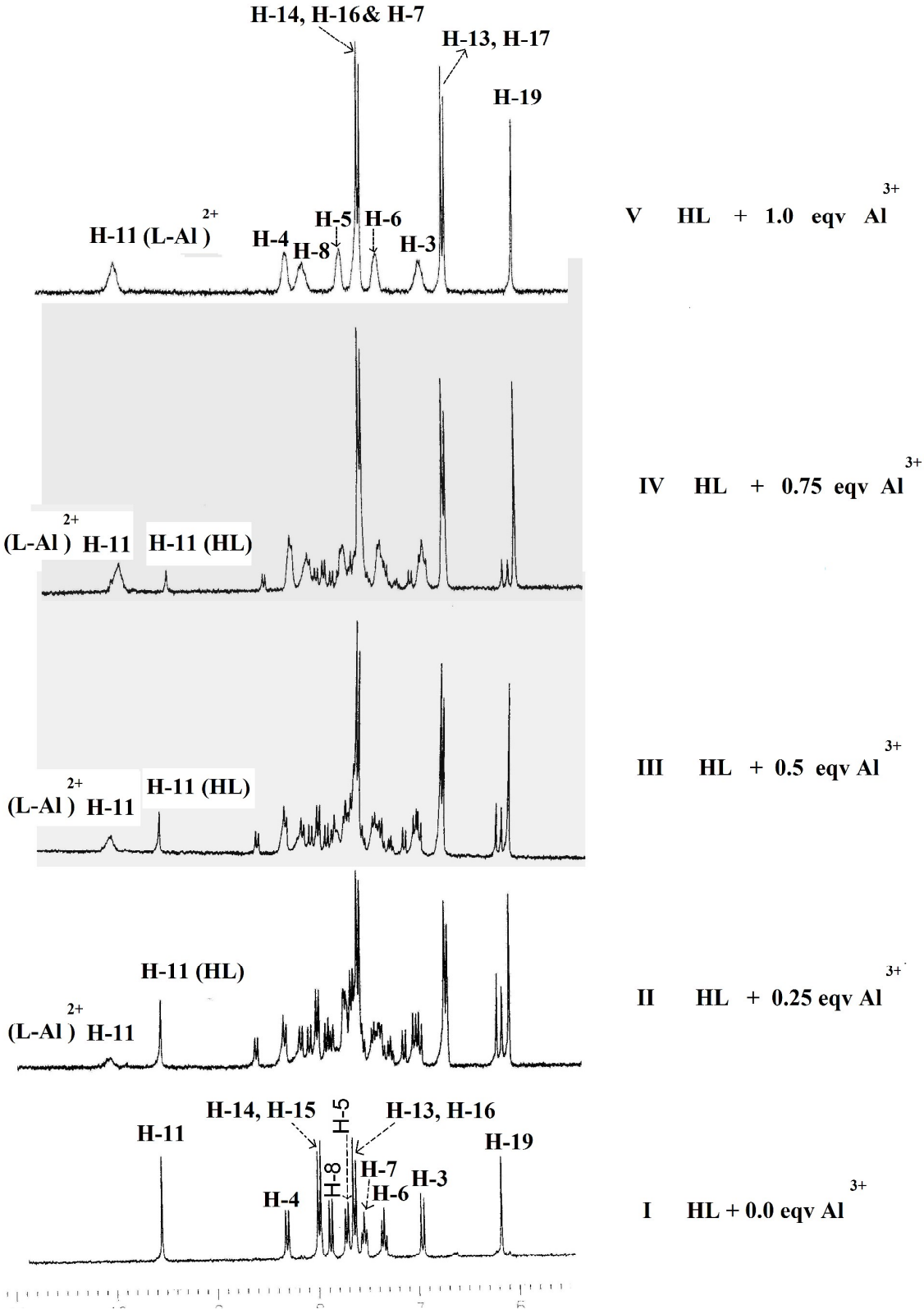

Fig.9. ^{1}H NMR titration of HL by Al^{3+} in CD_3OD at 294 K

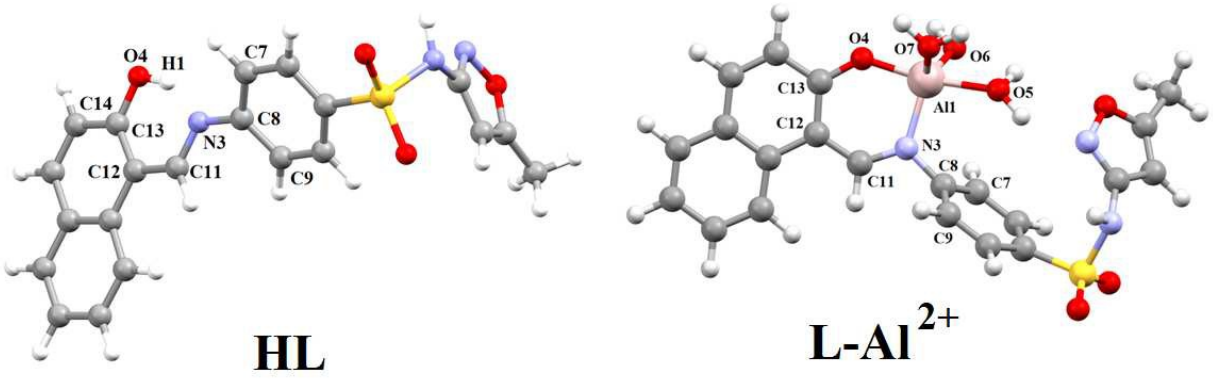

Fig.10. Optimized structure of HL and L-Al^{2+} by DFT/B3LYP 6-311g(d) method.

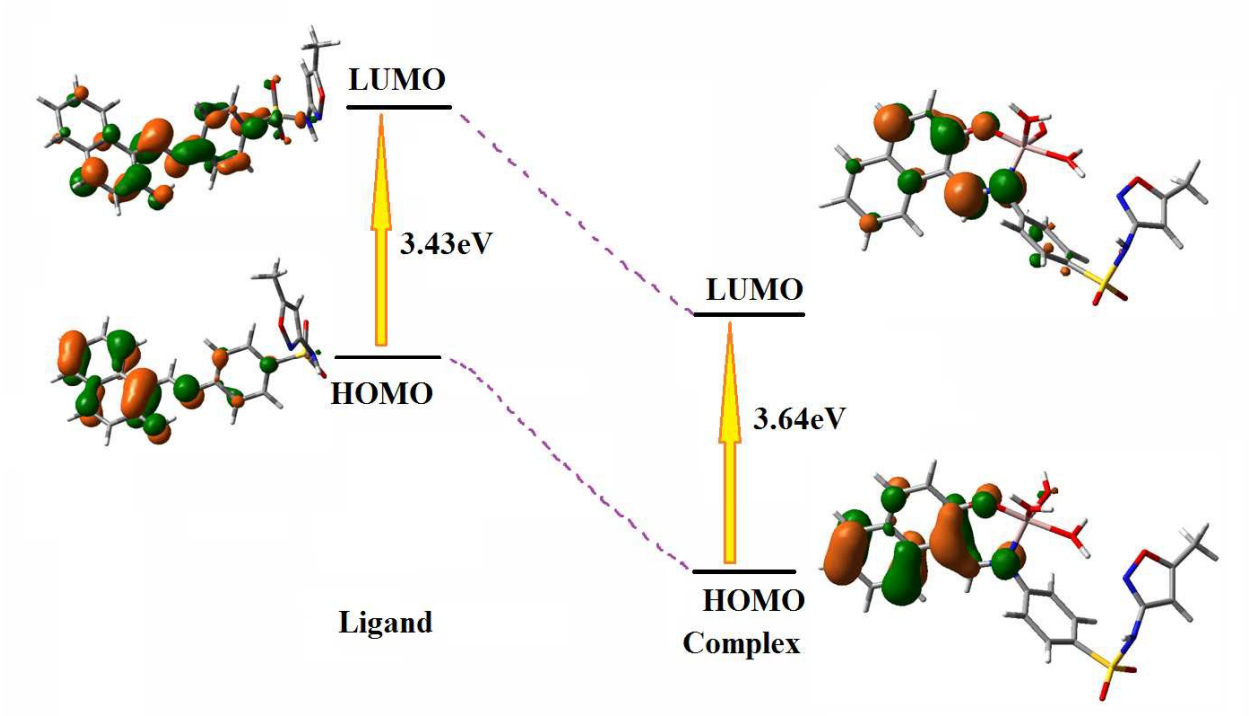

Fig.11. Frontier molecular orbital of HL and Al-L^{2+}

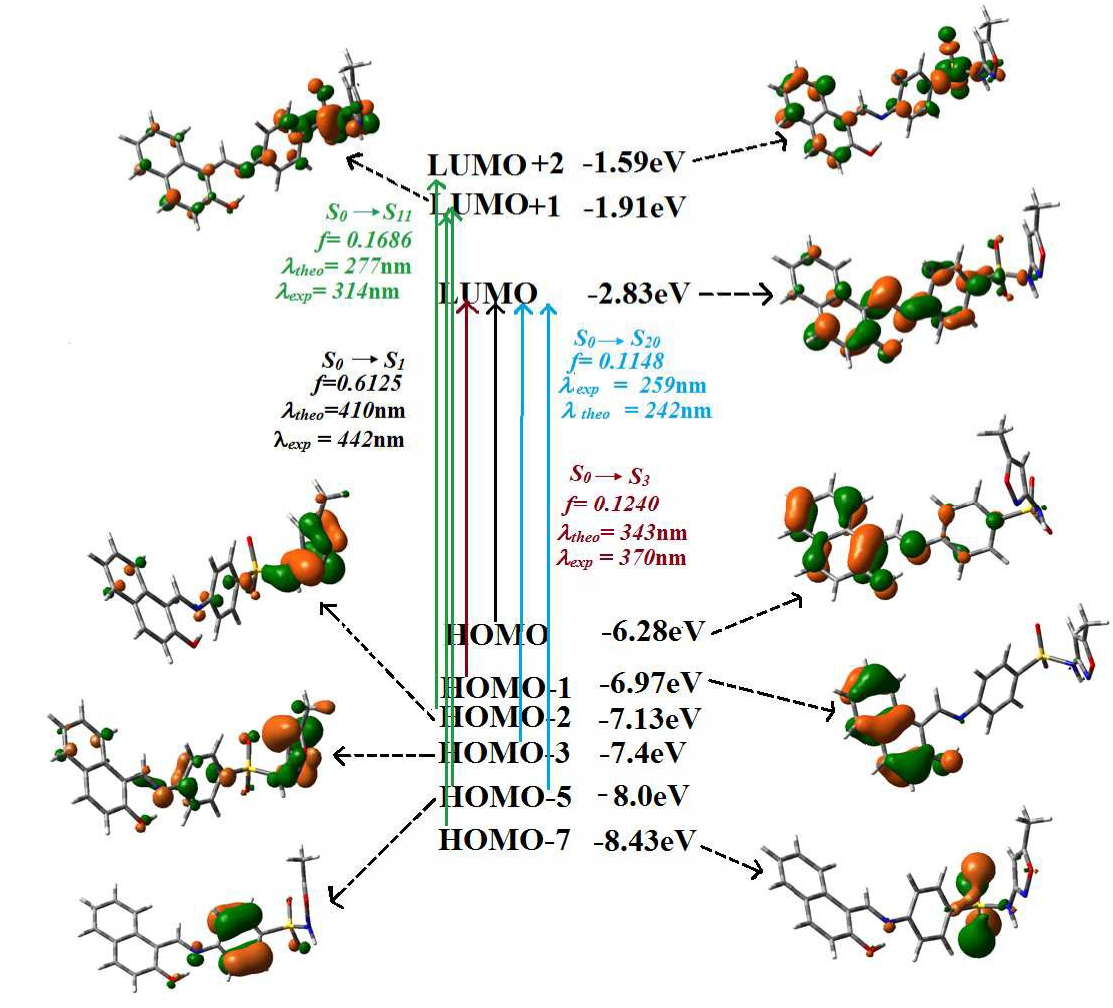

Fig.12. Frontier molecular orbitals involved in electronic transition in UV-Vis region of HL.

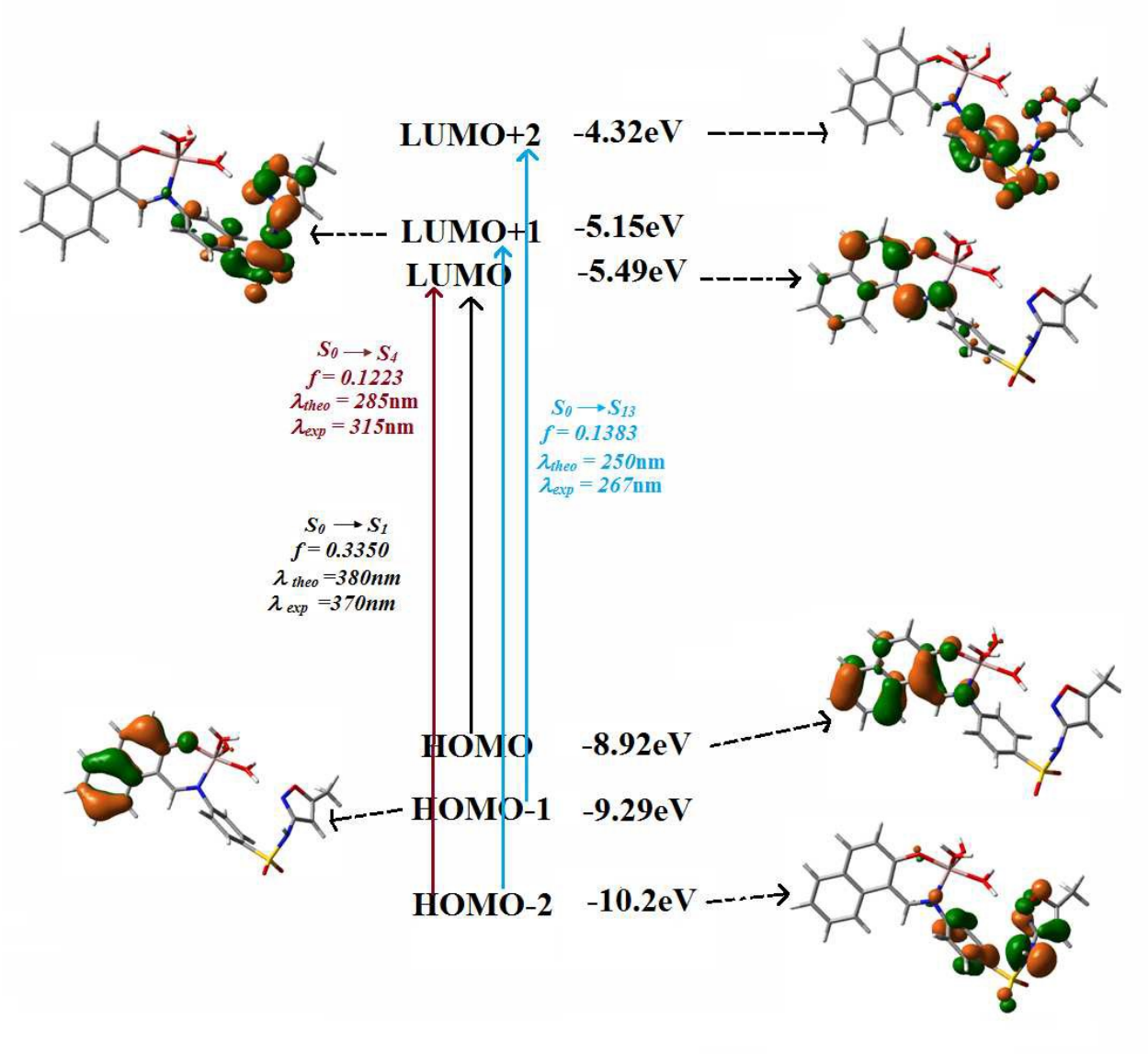

Fig.13. Frontier molecular orbitals involved in electronic transition in UV-Vis region of L-Al^{2+}.

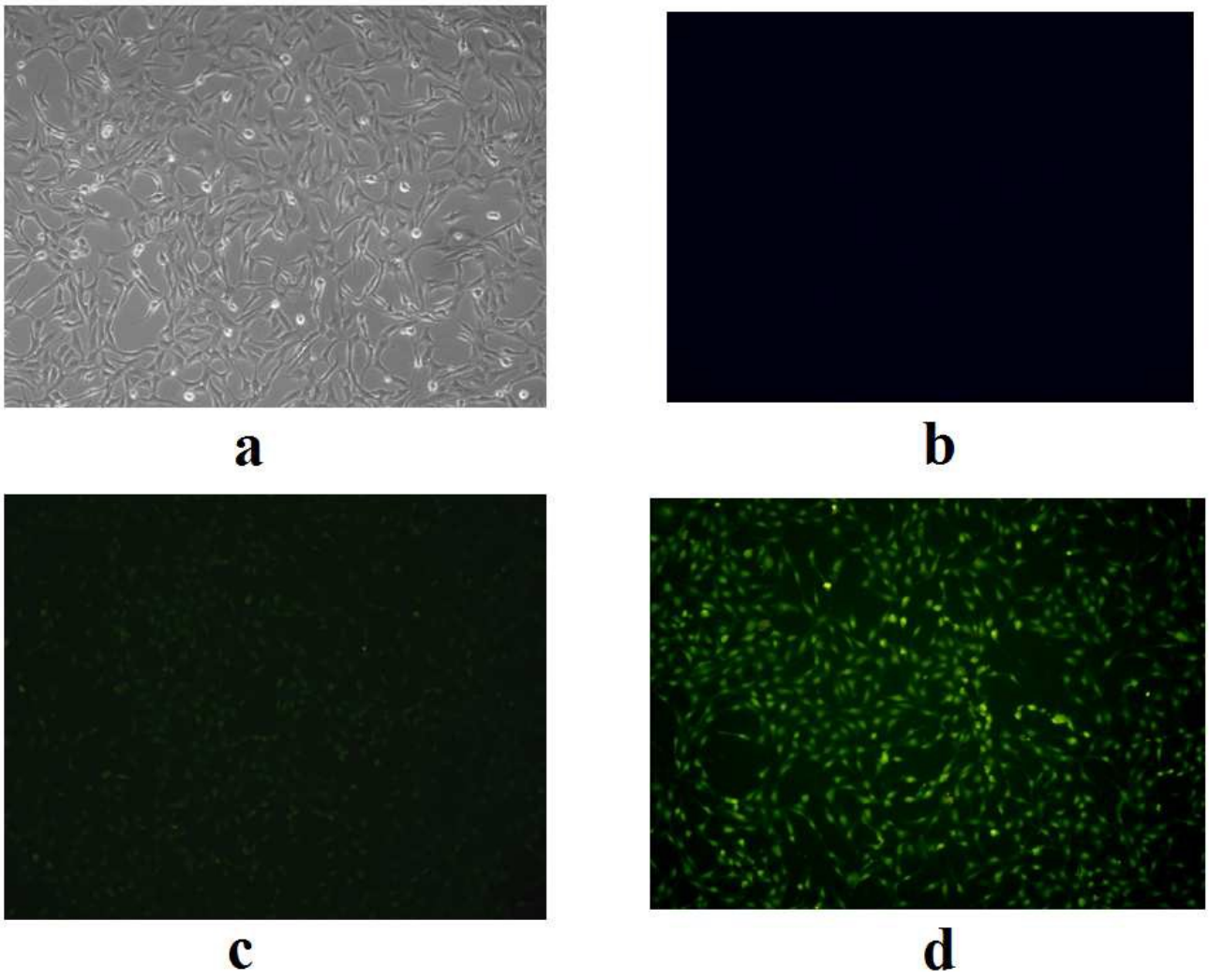

Fig 14. (a) Cell control, (b) Cell control in fluorescence microscope, (c) Cell in presence of HL, (d) Cell in presence of L-Al^{2+} complex.

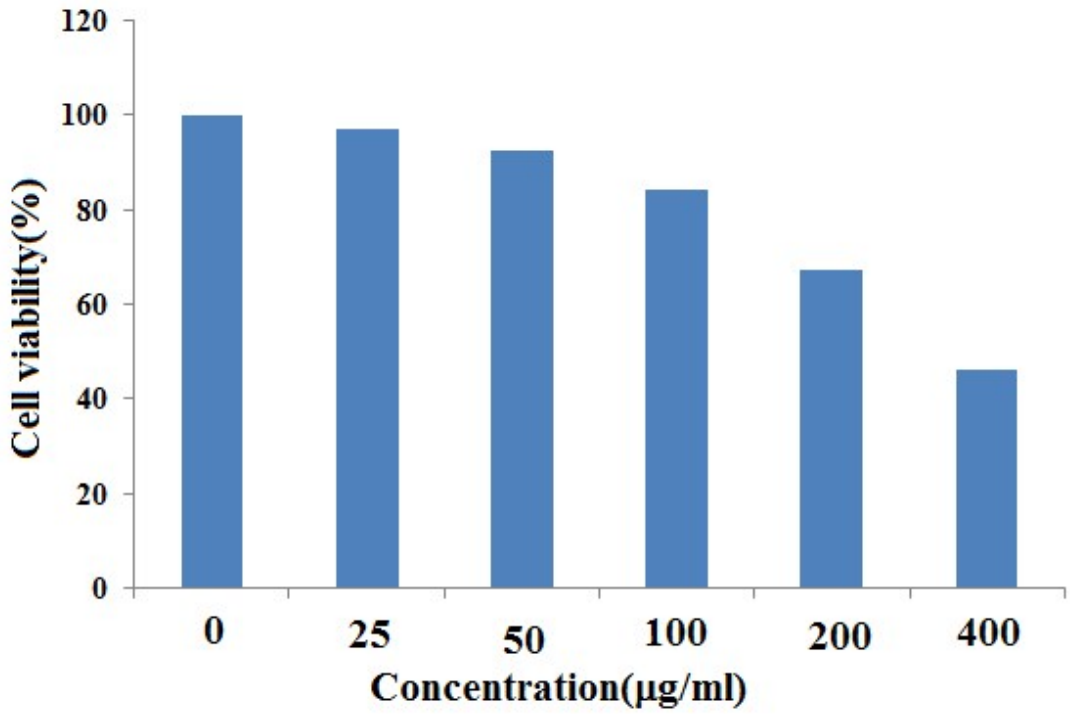

Fig.15. Cell viability data of HL.

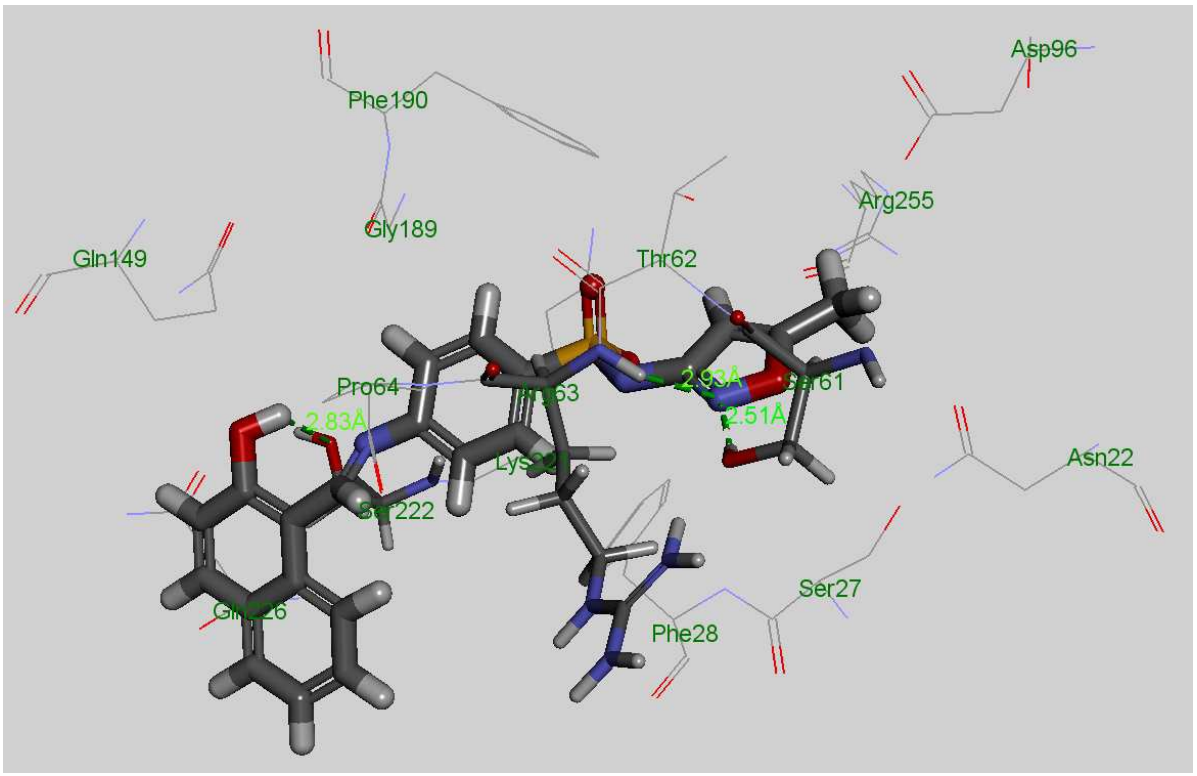

Fig.16. Best docked pose (2D) of HL inside the cavity of DHPS

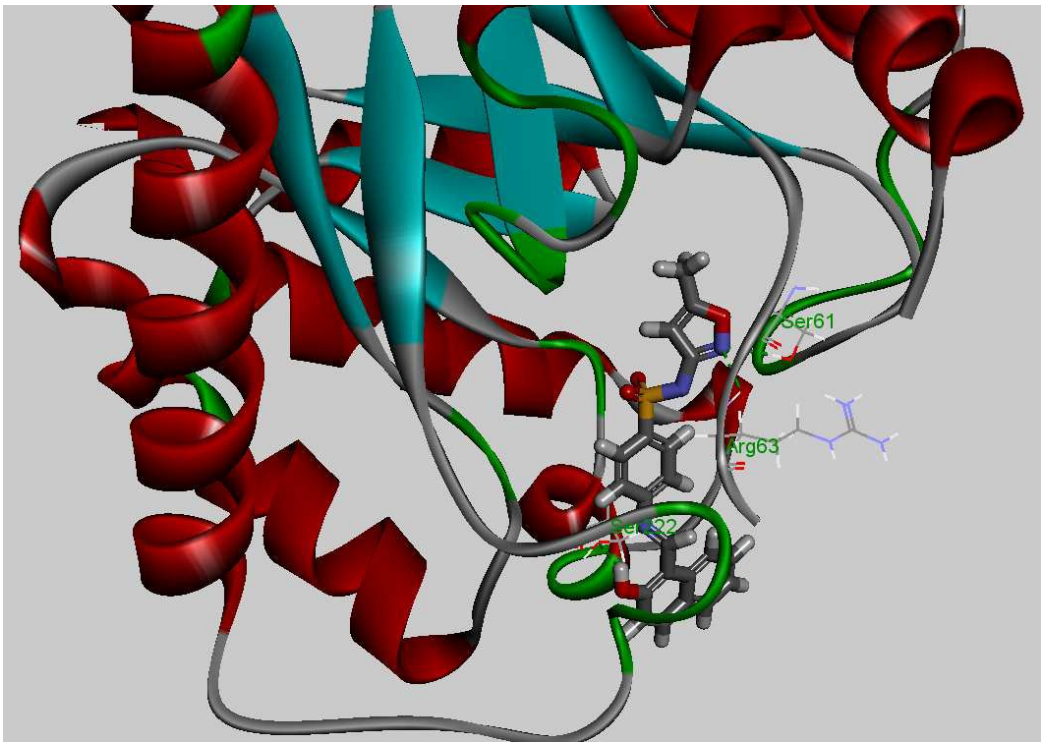

Fig.17. Best docked pose (3D) of HL inside the cavity of DHPS